USGS
science for a changing world

In cooperation with
New York City Department of Environmental Protection

Use of Advanced Borehole Geophysical Techniques to Delineate Fractured-Rock Ground-Water Flow, Faults, Foliation, and Fractures Along the Western Part of Manhattan, New York

Open-File Report 01-196

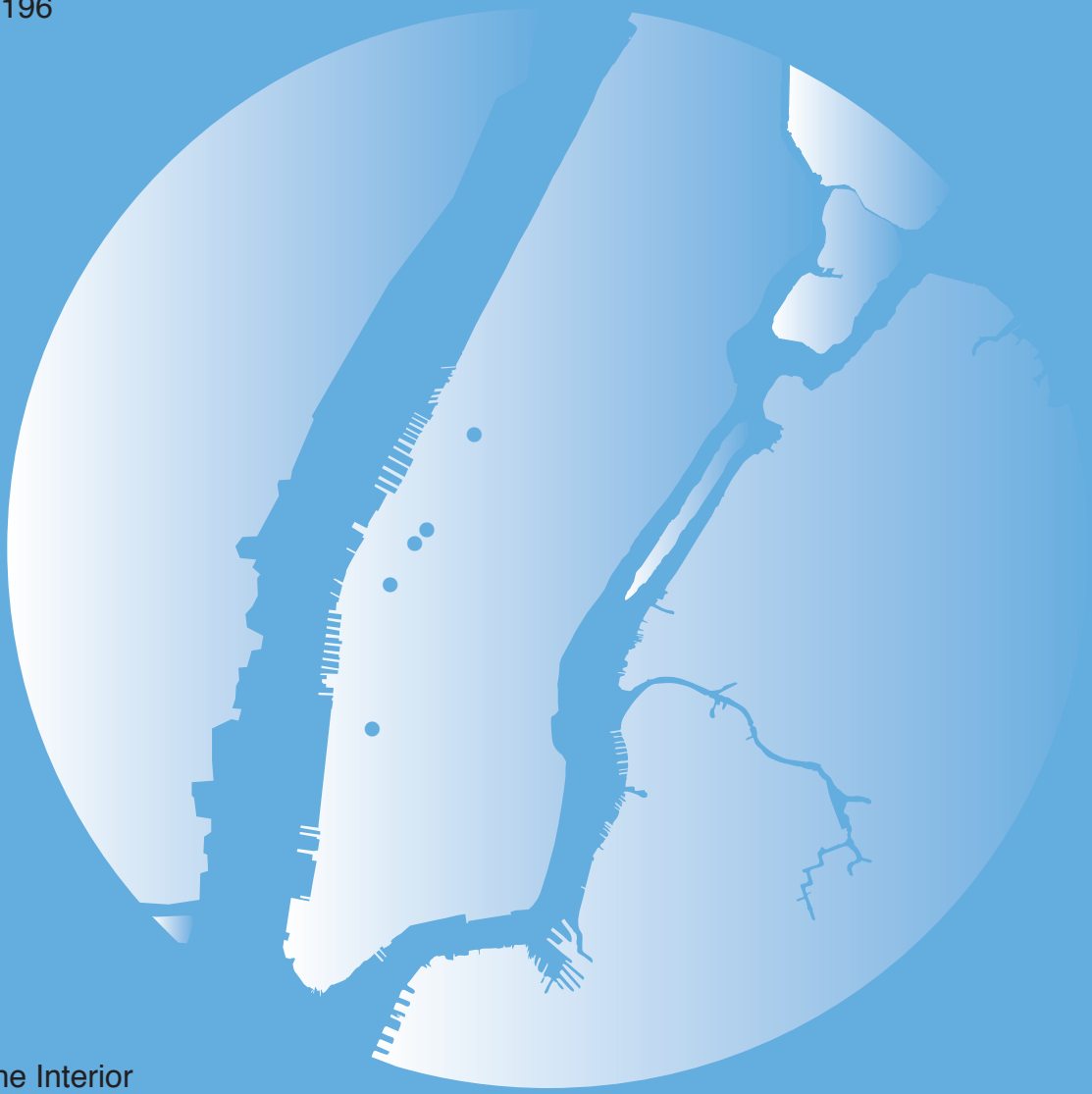

U.S. Department of the Interior
U.S. Geological Survey

Back of cover page is intentionally blank.

Use of Advanced Borehole Geophysical Techniques to Delineate Fractured-Rock Ground-Water Flow, Faults, Foliation, and Fractures along the Western Part of Manhattan, New York

By Frederick Stumm, Anthony Chu, and Andrew D. Lange

U.S. GEOLOGICAL SURVEY
Open-File Report 01-196

In cooperation with
NEW YORK CITY DEPARTMENT
OF ENVIRONMENTAL PROTECTION

Coram, New York
2001

U.S. DEPARTMENT OF THE INTERIOR
Gale A. Norton, Secretary

U.S. Geological Survey
Charles G. Groat, Director

The use of firm, trade, and brand names in this report is for identification purposes only and does not constitute endorsement by the U.S. Geological Survey.

For additional information
write to:

U.S. Geological Survey
2045 Route 112, Bldg. 4
Coram, NY 11727

Copies of this report may be
purchased from:

U.S. Geological Survey
Branch of Information Services
Box 25286, Bldg. 810
Denver, CO 80225-0286

CONTENTS

FIGURES

CONVERSION FACTORS, VERTICAL DATUM, AND ABBREVIATIONS

	Multiply By	To Obtain
Length		
inch (in.)	25.4	millimeter
inch (in.)	2.54	centimeter
foot (ft)	0.3048	meter
mile (mi)	1.609	kilometer
Area		
square mile (mi^2)	2.590	square kilometer
Flow		
gallons per minute (gal/min)	0.06309	liters per second
Transmissivity		
square foot per day (ft^2/d)	0.0929	square meter per day
Volume		
gallon per minute (gal/min)	3.785	liter per minute
Specific capacity		
gallon per minute per foot (gal/min)/ft	12.418	liter per minute per meter

Other abbreviations used in this report

greater than (>)
hour (h)
megahertz (MHz)
microsiemens per centimeter (µS/cm)
millisiemens per meter (mS/m)
minute (min)

Sea level: In this report, "sea level" refers to the National Geodetic Vertical Datum of 1929 (NGVD of 1929)--a geodetic datum derived from a general adjustment of the first-order level nets of the United States and Canada, formerly called Sea Level Datum of 1929.

Use of Advanced Borehole-Geophysical Techniques to Delineate Fractured-Rock Ground-Water Flow, Faults, Foliation, and Fractures along the Western Part of Manhattan, New York

By Frederick Stumm, Anthony Chu, and Andrew D. Lange

Abstract

Advanced borehole-geophysical methods were used by the U.S. Geological Survey in cooperation with the New York City Department of Environmental Protection (NYCDEP) to assess the geohydrology of crystalline bedrock at three test boreholes (W34ST-B, W37ST-A, and W55ST-A) on the western side of Manhattan Island, N.Y., in preparation for construction of a third water tunnel for New York City by the NYCDEP. The borehole-logging methods included natural gamma, single-point resistance, mechanical and acoustic caliper, focused electromagnetic induction, magnetic susceptibility, borehole-fluid temperature and resistivity, heat-pulse and EM (electromagnetic) flowmeter, borehole deviation, acoustic and optical televiewer, and borehole radar. The boreholes penetrated gneiss and other crystalline bedrock with an overall southwest-to-northwest dipping foliation. Most of the fractures encountered are either nearly horizontal or have moderate to high-angle northwest dip azimuths. Foliation within the tunnel-construction zone is southwest-to-northwest dipping, with fractures that average a northwest dip azimuth. EM and heat-pulse flowmeter logs obtained under pumping and ambient conditions, together with other geophysical logs, indicate transmissive fracture-flow zones in each borehole. The 60-megahertz directional borehole radar logs delineated the location and orientation of radar reflectors that would intersect the projection of the borehole above or below the drilled depth. Borehole data and interpretations may not reflect the exact location of the proposed tunnel-construction zone because of borehole deviation and constraints on borehole placement.

Fracture indexes range from 0.25 to 0.44 fracture per foot of borehole. The three-dimensional orientation of the fractures indicates a highly transmissive fracture zone at 328 to 330 feet below land surface (BLS) (-287.73 to -289.73 feet elevation) in W34ST-B that may intersect the proposed tunnel-construction zone to about 220 feet northwest of the borehole. Analysis of pumping tests of each borehole indicates that their total transmissivity ranges from 11 to 360 feet squared per day; the highest transmissivity is at the middle borehole (W37ST-A).

INTRODUCTION

In 1970, the New York City Department of Environmental Protection (NYCDEP) began construction of a third tunnel to supply water to New York City in the event that one of the two present water tunnels should require repair. Manhattan Island is about 12.5 mi long and 2 mi wide (fig. 1) and consists of unconsolidated deposits ranging from less than 1 ft thick to more than 200 ft thick overlying metamorphic bedrock. Manhattan Island is bounded on the west by the Hudson River, on the east by the East River, and on the south by New York Harbor.

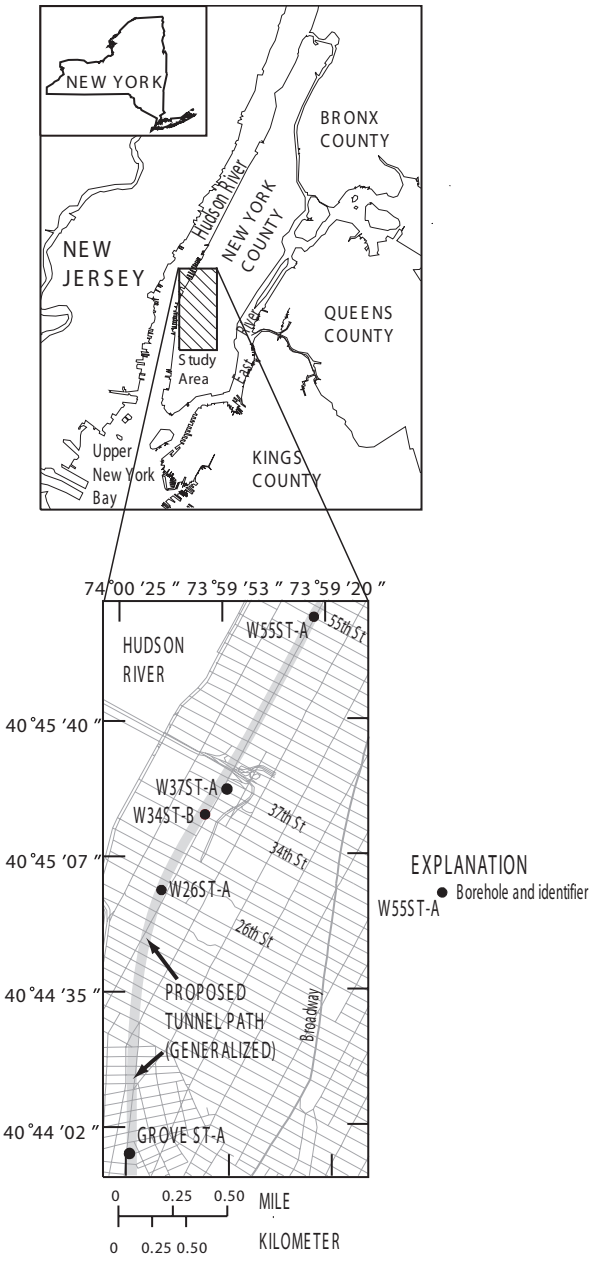

Figure 1. Locations of boreholes W34ST-B, W37ST-A, W55ST-A, W26ST-A, GroveST-A, Manhattan Island, N.Y.

Three test boreholes were drilled in 1998-99 to identify the type of rock and its degree of fracturing at the proposed tunnel depths, but the resulting information was insufficient in that (1) cores were not oriented, and (2) neither the hydraulic characteristics of fractures, nor the vertical deviation of the boreholes, can be determined from cores. Two additional boreholes were drilled, and only fracture and foliation orientations measured.

In 1998, the U.S. Geological Survey (USGS), in cooperation with the NYCDEP, began a study to apply advanced borehole-geophysical methods to provide a comprehensive geologic and hydrologic assessment of the crystalline bedrock in southeastern New York. These techniques were applied at the three boreholes on western Manhattan Island, N.Y., to identify (1) the bedrock lithology and major contacts, (2) the location and orientation (true strike and dip) of fractures and the foliation of the rock intersected by the boreholes, (3) the hydraulic characteristics of transmissive fracture-flow zones, and (4) major fractures or faults that lie as much as 100 ft beyond the borehole.

Purpose and Scope

This report (1) describes the geophysical methods used; (2) describes the geology at the three sites; (3) presents geophysical logs, equal-area plots of total-borehole and tunnel-zone fractures and foliation, and summarizes the geophysical interpretations of fractures, faults, and foliation in each borehole; (4) presents ground-water levels, water-temperature and resistance logs, and drawdown data; and (5) summarizes the transmissivity and locations of transmissive fractures in the boreholes, and relative hydraulic head. Borehole data and interpretations may not reflect the exact location of the proposed tunnel-construction zone because of borehole deviation and constraints on borehole placement.

Borehole-Geophysical Logging Methods

Borehole-geophysical logs collected in this investigation included natural gamma, single-point-resistance, mechanical and acoustic caliper, focused electromagnetic induction, magnetic susceptibility, borehole-fluid temperature and resistance, heat-pulse and EM flowmeter, borehole deviation, acoustic and optical televiewer, and borehole radar. The logging methods are briefly described below.

Natural-gamma (gamma) logs are a record of the total gamma radiation detected in a borehole (Keys, 1990) and are most commonly used for lithologic and stratigraphic correlation. Radioiso-

topes in bedrock minerals such as feldspar and mica are instrumental in correlating lithology. Clay minerals within fractures may be detected as elevated gamma responses in comparison with those of surrounding rock.

Spontaneous-potential (SP) logs provide a record of the naturally occurring potential difference along the borehole and can be used to identify changes in lithology, bed thickness, and salinity of formation water under some geologic conditions (Keys, 1990).

Single-point resistance (SPR) logs provide a measure of the electrical resistance of the rock or formation, in ohms, and are used to obtain qualitative lithologic information with a depth resolution approximately equal to borehole diameter (Keys, 1990).

Caliper logs provide information on lithology and the location of major fractures or faults. Mechanical calipers use spring-loaded arms to profile the surface of the borehole wall. Acoustic calipers calculate the distance to the borehole wall from the traveltime of the acoustic signal emitted from an acoustic televiewer (ATV) to provide high-resolution, compass-oriented logs (Keys, 1990).

Focused electromagnetic induction (EM) logs provide a profile of the electrical conductivity of the rock around the borehole with respect to depth, which can be interpreted in terms of formation water conductivity. This technique uses an electromagnetic emitter coil to induce electrical eddy currents within a specified volume of the surrounding formation to generate a secondary electromagnetic field. The intensity of the secondary field received by the receiver coil is proportional to the formation's conductivity (Keys, 1990; Serra, 1984; Keys and MacCary, 1971).

Magnetic-susceptibility (MAG) logs provide a record of the variations in magnetic minerals within the surrounding rock. Magnetite is the most common magnetic mineral, and local variations in its abundance may indicate lithologic contacts (McNeill and others, 1996).

Temperature logs measure the temperature of the fluid column as a function of depth and can provide information on the movement of ground water through the borehole and the location of areas that produce or accept water (Keys, 1990).

Borehole fluid resistivity logs of ground water in a borehole provide a record of the capacity of the fluid to conduct electricity and provide an indication of salinity (Keys, 1990).

Heat-pulse/EM flowmeter logs measure vertical flow in boreholes and can indicate which fractures are producing or accepting water in a borehole under pumping and static conditions (Keys, 1990). Cross-borehole flowmeter tests can be used to identify connections between fractures (Paillet, 1998).

Acoustic televiewer (ATV) uses a rotating transducer that transmits and receives high-frequency acoustic pulses to produce an image of the intensity of acoustic energy reflection. The ATV provides high-resolution information on the location and strike and dip of fractures or faults within a borehole (Keys, 1990; Williams and Johnson, 2000).

Borehole-deviation logs provide information on the borehole's angle and direction of deviation from vertical. All deep boreholes deviate from vertical; therefore, deviation logs must be obtained before three-dimensional information on fractures and faults is interpreted (Keys, 1990). After processing, the resulting log indicates the true depth of the borehole, its distance from vertical, and the direction or azimuth of deviation.

Optical televiewer (OTV) digitally records a high-resolution optical scan of the borehole wall that can be used to produce a virtual core. The virtual core is oriented to allow for visualization of major faults and fractures as they were imaged within the borehole. Faults and fractures, both opened and sealed, can be viewed in three-dimensional orientations. This system also allows measurement of true strike-and-dip orientation and fracture spacing (Stumm and others, 2000; Williams and Johnson, 2000).

Borehole radar uses a single-hole, 60-MHz directional radar unit (transmitter/receiver) that can detect fracture zones and other structural features at distances to as much as 100 ft from the borehole in electrically resistive rocks. The data logs can be used to calculate the orientation of fractures (Singha and others, 2000).

Borehole Network

Five NX-sized (3-in diameter) boreholes (W34ST-B, W37ST-A, W55ST-A, W26ST-A, and GroveST-A) were drilled by the diamond-core method to obtain continuous rock core samples from the west side of Manhattan (fig. 1), the proposed area of the new tunnel. All boreholes were cased with steel from land surface through the unconsolidated overburden to the top of bedrock, and were uncased or open from the bedrock surface to the bottom of the drilled depth. The full suite of geophysical logs was not completed at boreholes W26ST-A or GroveST-A; fracture and foliation data were collected from W26ST-A and GroveST-A, but no other analyses were completed (see appendix). Boreholes W34ST-B, W37ST-A, and W55ST-A were drilled to depths of 625.7, 651.4, and 619.4 ft below land surface (BLS), respectively (-585.43, -610.09 and -579.99 ft elevation).

Acknowledgments

The authors thank the USGS Office of Ground Water and Branch of Geophysical Applications and Support for technical assistance and cooperation, the USGS Borehole Geophysics Research Project for technical assistance, and members of the Geotech Unit of the NYCDEP Waterworks Construction Section for technical assistance.

GEOHYDROLOGY

Manhattan's west side is underlain by high-grade metamorphic bedrock consisting of a sequence of gneiss and schistose-gneiss interlayered with granite (Baskerville, 1992). The bedrock contains many fractures, some of which are transmissive. Depth to bedrock ranges from 8 to 34 ft BLS (32.27 to 5.41 ft elevation).

The ATV, OTV, and borehole-radar data indicate that all boreholes penetrate moderately fractured rock that contains highly fractured zones. Every borehole contains medium and large open fractures that were transmissive. Structural trends of these geologic units imply that all fractures and faults detected in each borehole extend beyond each borehole. The gamma, SPR, EM-conductivity, resistivity, fluid-temperature, and resistance logs detected some of the fracture zones.

Methods of Geologic-Structure Analysis

Foliation and fractures encountered in each borehole were delineated from the OTV and ATV geophysical data. Fractures were classified as small, medium, large, or very large, depending on the apparent aperture or width of the opening. Measured fracture apertures in the boreholes are considered apparent to account for alterations caused by the drilling process. Small fractures or microfractures have apertures of 0.04 in. (1 mm) or less; medium fractures have apertures of >0.04 to 0.39 in. (>1 to 10 mm); large fractures have apertures >0.39 to 9.8 in. (>10 to 25 cm); and very large fractures have apertures >9.8 in. (>25 cm). Borehole-radar data were used to (1) verify the assumption that most fractures extend beyond the borehole, (2) detect major fractures or faults as far as 100 ft from the borehole that may not intersect any borehole in the area and would otherwise had been missed, and (3) delineate the orientation (strike and dip) of these distant fractures or faults.

Orientations of each fracture in each borehole was calculated from the ATV and OTV data through standard computer programs. Deviation from vertical and magnetic declination of each borehole was included in the final orientation calculation. Final corrected orientation of fractures and foliation was listed as dip azimuth and dip angle (dip). Orientation of all fractures is listed in the appendix.

The orientations were then converted through standard equal-area net projections as poles to planes, where dip azimuths have 180° added, and dip-plunge angles are subtracted from 90°. Computer-generated stereonet contours were used to identify fracture or foliation populations and their mean orientations. The mean fracture or foliation orientation (strike and dip) is the average for the entire cluster of features plotted.

The tunnel-construction zone (TCZ) was defined as a horizon ranging from 50 ft above the roof of the proposed tunnel to 50 ft below the tunnel floor; this zone represents the interval from 540 to 625.7 ft BLS (-499.73 to -585.43 ft elevation) at W34ST-B, 530 to 651.4 ft BLS (-488.68 to -610.09 elevation) at W37ST-A, and from 462 to 619.4 ft BLS (-422.59 to -579.99 elevation) at W55ST-A. Most boreholes are deeper than the bottom of the TCZ. High-angle large fractures above the TCZ at each of the boreholes, if continuous, could intersect the TCZ at a distance and were considered to be critical features. For this reason, fracture analysis of the entire borehole is most useful

in terms of potential intersections with the tunnel away from the borehole. Within the TCZ, fracture and foliation data are useful for the borehole location only.

Structure orientations for fractures or foliation are displayed further on as "tadpoles," which are circles with "tails" plotted with respect to a horizontal scale to indicate the degree of dip-plunge angle of the structures from 0 to 90°. The tail of each tadpole points to the dip azimuth of the structure. The tadpole plots of foliation and fractures are included with the geophysical logs for each borehole to illustrate the variation in dip azimuth and dip with depth.

Analysis of the fractures within each borehole included the fracture index. The total number of fractures detected in each borehole was divided by the thickness of bedrock encountered to provide a fracture index indicating the average number of fractures per foot of bedrock. Average fracture indexes at W34ST-B, W37ST-A, and W55ST-A were 0.44, 0.40, and 0.25 fracture per foot of bedrock, respectively.

Foliation

Foliation analyses, grouped by depth, indicate populations with similar dip azimuths and dip angles. Total borehole-foliation dip azimuths are southwestward at W34ST-B, and northwestward at W37ST-A and W55ST-A. Total borehole foliation at W34ST-B, W37ST-A, and W55ST-A is N09°W57°SW, N06°E55°NW, and N16°E60°NW, respectively.

Foliation data from within the TCZ indicate a change from a 65° southwest dip at W34ST-B to a 58° northwest dip at W37ST-A, and a 61° northwest dip at W55ST-A. This variation in dip angle and azimuth if present at the proposed tunnel-construction zone could create block- or wedge-failure during tunnel construction.

Fractures

Fracture analysis identifies populations with similar dip azimuths and dip angles. No general correlation between fracture orientation and depth is evident in the study area. Overall total borehole fracture-population orientations are (1) nearly horizontal, and (2) moderate to high-angle dip with a northwest dip azimuth. The intersection of these fracture populations, coupled with the spatial variation in foliation dip azimuth, could create block- or wedge-failure during tunnel construction. Fracture means have dips of 17° to the northwest at W34ST-B, an 8° dip to the northwest at W37ST-A, and a 44° dip to the northwest at W55ST-A. Many fractures were detected throughout the study area with dip angles in excess of 70°. The appendix lists fracture depth, dip azimuth, and dip angle of all fractures observed by OTV within the three boreholes. Analysis of the 60-MHz directional radar indicates strong radar reflectors that are probably fractures that, if transmissive, could produce appreciable quantities of ground-water to flow into the tunnel.

Methods of Ground-Water Flow Analysis

Ground-water levels were measured at three (W34ST-B, W37ST-A, W55ST-A) boreholes during field visits from November 1998 through April 1999. Fluid-temperature, resistance, and flowmeter logs were collected at each borehole (except W55ST-A) during pumping and ambient conditions (fig. 2). Measurements of the drawdown, pumping rate, and total pumping time at each borehole during test pumping were applied to a computer program (Bradbury and Rothschild, 1985) to calculate specific capacity and transmissivity of the entire borehole.

Fluid-temperature and resistance logs were used to help delineate transmissive fractures within the boreholes. Erratic and abnormal temperature gradients can be caused by ground-water flow into or out of fractures intersected by the boreholes (Keys, 1990; Williams and Conger, 1990). Changes in fluid resistance also may occur at transmissive fractures.

Transmissivity

Calculated transmissivity values for boreholes W34ST-B, W37ST-A, and W55ST-A were 75, 362, and 11 ft^2/d, respectively. Clearly, the transmissive fracture network is a discrete system not correlated specifically with the fracture index. Several fractures were found to be highly transmissive and could produce appreciable quantities of ground water to flow into the tunnel during construction.

The flowmeter logs were analyzed through techniques of Paillet (1998, 2000), whereby differences between flow values at adjacent fracture zones within each borehole are attributed to measurement scatter and a possible net difference in borehole flow. Therefore, flow-log interpretation involves identification of the relative amounts of inflow or outflow occurring at

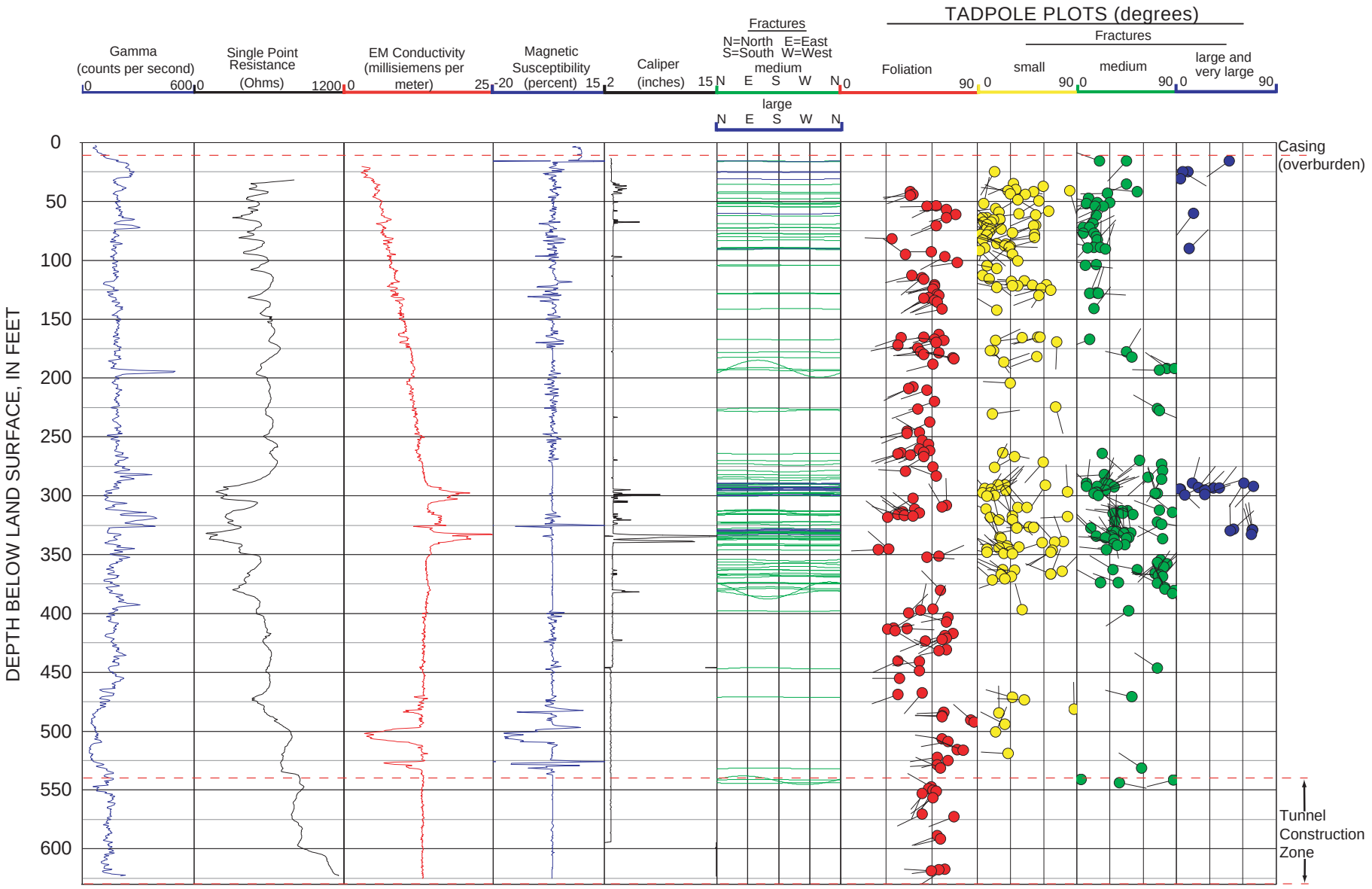

Figure 2. Suite of borehole-geophysical logs from borehole W34ST-B, Manhattan Island, N.Y., 1998. (Borehole location is shown in fig. 1.)

specific depth intervals. Inflow or outflow at several depth intervals at each borehole was measured; each of these intervals coincides with a fracture, or sets of fractures. The effects of hydraulic-head differences between zones can be eliminated by analyzing flow under ambient and pumping conditions in accordance with the techniques of Molz and others (1989) and Paillet (2000).

Ground-Water Levels in Fall 1999 and Summer 2000

Water levels in the fractured bedrock averaged 29.1 ft elevation in the northern part of the study area at W55ST-A, 13.5 ft elevation at W37ST-A, and 10.5 ft elevation in the southern part at W34ST-B. The hydraulic head in fractured bedrock wells represents the transmissivity-weighted average of the heads in all transmissive fractures in the borehole, rather than head in specific fractures.

DELINEATION OF FAULTS, FRACTURES, FOLIATION, AND GROUND-WATER FLOW

Faults, fractures, and foliation were interpreted from OTV, ATV, borehole-radar, gamma, SP, SPR, EM, MAG and caliper logs, which are reproduced in the individual borehole summaries that follow. The SP log yielded no significant results as a result of the conditions of the borehole and therefore is not discussed further. The hydraulic characteristics of the bedrock at each borehole are described in the summaries. OTV data (borehole depth, fracture orientation, and foliation orientation) for all fractures and faults in all five boreholes are listed in the appendix.

The following borehole summaries describe results of the fault, fracture, and foliation data analysis and the ground-water flow zones for boreholes W34ST-B, W37ST-A, and W55ST-A. Gamma, SPR, EM, MAG, and caliper logs with tadpole plots of the foliation and fractures from OTV data for each borehole are depicted in figures 2, 7, and 11; equal-area plots of total borehole and TCZ fractures and foliation are depicted in figures 3, 8, and 12; deviation plots for each borehole are depicted in figures 4, 9, and 13; and an example of a directional radar log showing a major reflector is presented in figure 5.

Borehole W34ST-B

W34ST-B is the first of five boreholes geophysically logged within the proposed westside tunnel (fig. 1). The borehole was drilled to a depth of 625.7 ft BLS (-585.43 ft elevation), with steel casing extending from land surface (40.27 ft elevation) to 8.0 ft BLS (32.27 ft elevation) in the unconsolidated deposits (overburden). The bedrock penetrated by the borehole consists of a sequence of gneiss and schistose gneiss with granite.

Faults, Fractures, and Foliation

The ATV and OTV data indicate a total of 271 small, medium, and large fractures from below the casing to the bottom of the borehole (shown as fracture and foliation logs in fig. 2 and listed in appendix). Large open fractures were detected at 16, 25, 31, 60, 90, 289, 292, 299, 300, 329, 330 and 332 ft BLS (24.27, 15.27, 9.27, -19.73, -49.73, -248.73, -251.73, -258.73, -259.73, -288.73, -289.73 and -291.73 ft elevation). In addition, four very large open fractures represent a possible fault-gouge zone from 328 to 330 ft BLS (-287.73 to -289.73 ft elevation, fig. 2). This gouge zone is highly fractured and has a horizontal diameter of almost 30 in. The borehole has a fracture index of 0.44 fracture per foot of borehole. The tadpole plots of fractures (fig. 2) indicate a high fracture density at depths from 30 to 125 ft BLS (10.27 to -84.73 ft elevation) and from 275 to 375 ft BLS (-234.73 to -334.73 ft elevation). The majority of small and large fractures have dip angles less than 45°. No clear pattern of dip azimuth orientations with respect to depth is evident from in the tadpole plots of fractures. The mean fracture orientation for the 271 fractures is N20°E17°NW (fig. 3). About 12 high-angle fractures with dip angles greater than 70° were encountered throughout the length of the borehole. Fractures within the proposed TCZ, which extends from 540 ft BLS (-499.73 ft elevation) to the bottom of the borehole (fig. 3), were analyzed. All fractures from 370 ft BLS (-329.73 ft elevation) to the bottom of the borehole were included to provide a statistically significant sample. In all, 24 fractures were detected, 14 of which are medium size. The mean fracture orientation for the TCZ is N34°E39°NW (fig. 3).

The tadpole plots of foliation (fig. 2) indicate correlations between foliation, azimuth, dip angle, and depth. The foliation dip azimuth in most of the bore-

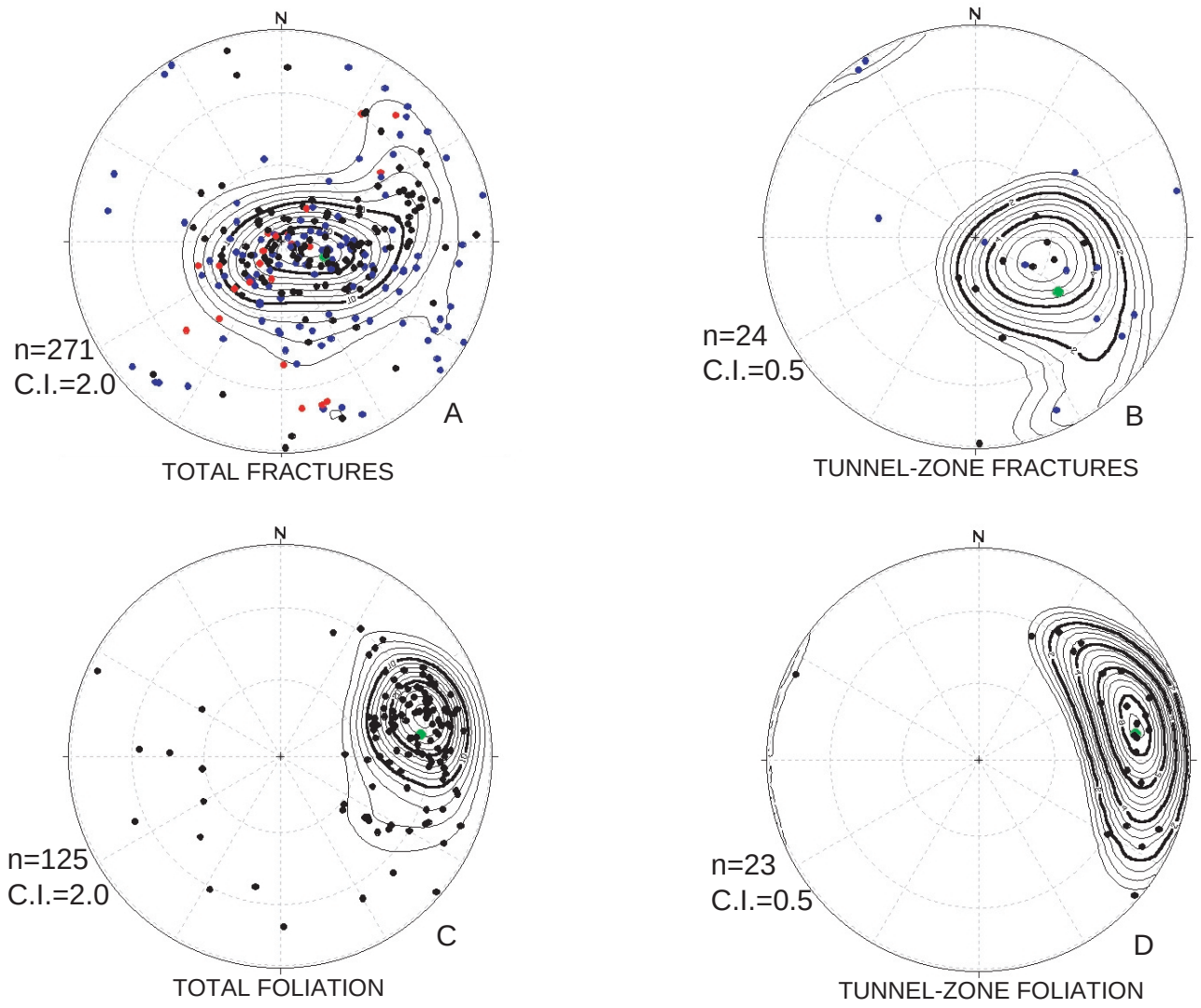

Figure 3. Stereonet plots of borehole W34ST-B, Manhattan Island, N.Y., 1998: A. Total fractures. B. Tunnel-zone fractures. C. Total foliation. D. Tunnel-zone foliation. (Borehole location is shown in fig. 1.)

hole is southwestward, except in a zone from 350 to 420 ft BLS (-309.73 to -379.73 ft elevation), where it is northeastward. The foliation dip angle increases slightly with depth. The mean orientation of foliation for the entire borehole is N09°W57°SW (fig.3). The TCZ foliation was analyzed from 50 ft above the projected tunnel ceiling (invert) to the bottom of the borehole. The mean TCZ foliation is N09°W65°SW (fig.3).

The gamma-log analysis (fig. 2) indicates fairly uniform gamma counts in the bedrock, except for a few spikes that reflect possible changes in mineralogy. The SPR log (fig. 2) has conductive spikes at locations that correlate with large fractures; the spikes may indicate chemically weathered zones (clays) and also ground-water in some fractures. The SPR and EM log data indicate the upper 300 ft of the rock to be more conductive than the rest. Two zones at 290 to 300 ft BLS (-249.73 to -259.73 ft elevation) and 328 to 335 ft BLS (-287.73 to -294.73 ft elevation) have the lowest resistance and the highest EM conductivity in the borehole (fig. 2) and correlate with two highly fractured transmissive zones. The magnetic-susceptibility log (fig. 2) shows areas of low response that indicate granitic zones or other areas containing low concentrations of magnetite. The lowest 85 ft of the borehole is mostly granitic.

Borehole-deviation analysis of W34ST-B indicates the bottom of the borehole to be a horizontal distance of 79.6 ft from its surface starting point at an azimuth of 84° (fig. 4). The true vertical depth of the borehole is calculated to be 618.2 ft BLS (-577.93 ft elevation).

Borehole radar data indicate six reflectors (possibly fractures) beyond the borehole, with orientations of N156°E85°NE, N143°W80°SE, N77°E53°NW, N77°E54°NW, N23°W75°SW, and N23°W88°SW (fig. 5).

Ground-Water Flow Zones

The lowest hydraulic heads of all three boreholes were in W34ST-B, probably as a result of proximity to the Hudson River (about 2,500 ft), and the relatively long distance from Manhattan Island's topographic high to the northeast. Water-level fluctuations of about 4 ft during successive field visits over 2 months indicate a possible tidal (Hudson River), pumping, or natural recharge effect.

EM-flowmeter, fluid-temperature, fluid-resistance logs from borehole W34ST-B (fig. 6) indicate several depth intervals at which a deflection or change in slope corresponds to transmissive fractures. Slope changes in these logs are seen at 72, 299, 328 to 330, 355 to 363, and 470 ft BLS (-31.73, -258.73, -287.73 to -289.73, -314.73 to -322.73, and -429.73 ft elevation, fig. 6). OTV images of two medium fractures at 72 ft BLS (-31.73 ft elevation) show mineral streaking that suggests ground-water outflow. Small deflections in the fluid-temperature and resistance logs are seen at 72 ft BLS (-31.73 ft elevation, fig. 6).

Pumping the borehole at a rate of 3 gal/min for 2.88 h produced a drawdown of 11.2 ft, or a specific capacity of 0.27 (gal/min)/ft. Total borehole transmissivity was calculated to be 75 ft^2/d. EM flowmeter, fluid-temperature, and fluid-resistance logging detected five separate transmissive fracture zones within the borehole at 72, 299, 328 to 330, 355 to 363, and 470 ft BLS (-31.73, -258.73, -287.73 to -289.73, -314.73 to -322.73, and -429.73 ft elevation, fig. 6). Although somewhat ambiguous, the analysis of ambient ground-water conditions indicate a small amount of downflow between the 72-ft and 328 to 330 ft BLS (-31.73-ft and -287.73 to -289.73-ft elevation) fracture zones. Under pumping conditions, 75 percent of the borehole's transmissivity corresponds to the 299-ft BLS (-258.73 ft elevation) zone, and 25 percent to the 72-ft BLS (-31.73-ft elevation) zone. Fluid-log analysis of ambient and pumping conditions also indicates upward ambient flow from the 299-ft BLS (-258.73-ft elevation) zone to the 72-ft BLS (-31.73-ft elevation) zone, and downward flow from the 300-ft BLS (-259.73-ft elevation) zone to the 328- to 330-ft BLS (-287.73- to-289.73-ft elevation) zone. Transmissivity values for the 72-ft and 299-ft BLS (-31.73-ft and -258.73-ft elevation) fracture zones were 19 and 56 ft^2/d, respectively.

If intersected, the 328- to 330-ft BLS (-287.73- to -289.73-ft elevation) fracture zone may result in appreciable quantities of ground water to flow into the tunnel because of high transmissivity and large open fractures. This zone had a reported low Rock Quality Designation (RQD) during drilling (NYCDEP, oral commun., 1998). RQD is a percentage value obtained by dividing the summed lengths of all core pieces equal to or greater than 4 in. long by the cored interval length. Trigonometric analysis of the dip angles and

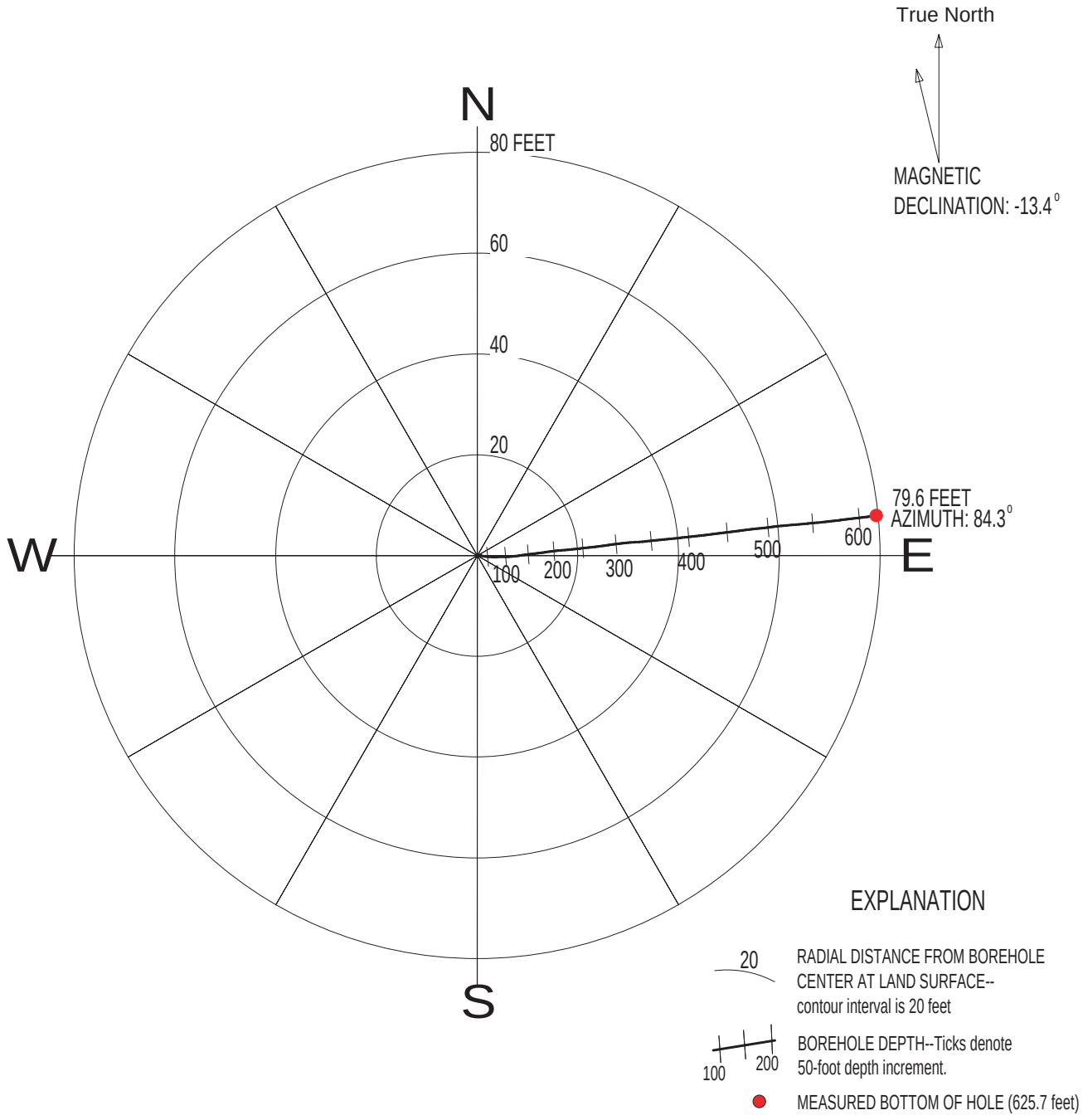

Figure 4. Deviation plot of borehole W34ST-B, Manhattan Island, N.Y., November 1998. (True depth of the borehole is 618.2 feet. Borehole location is shown in fig. 1.)

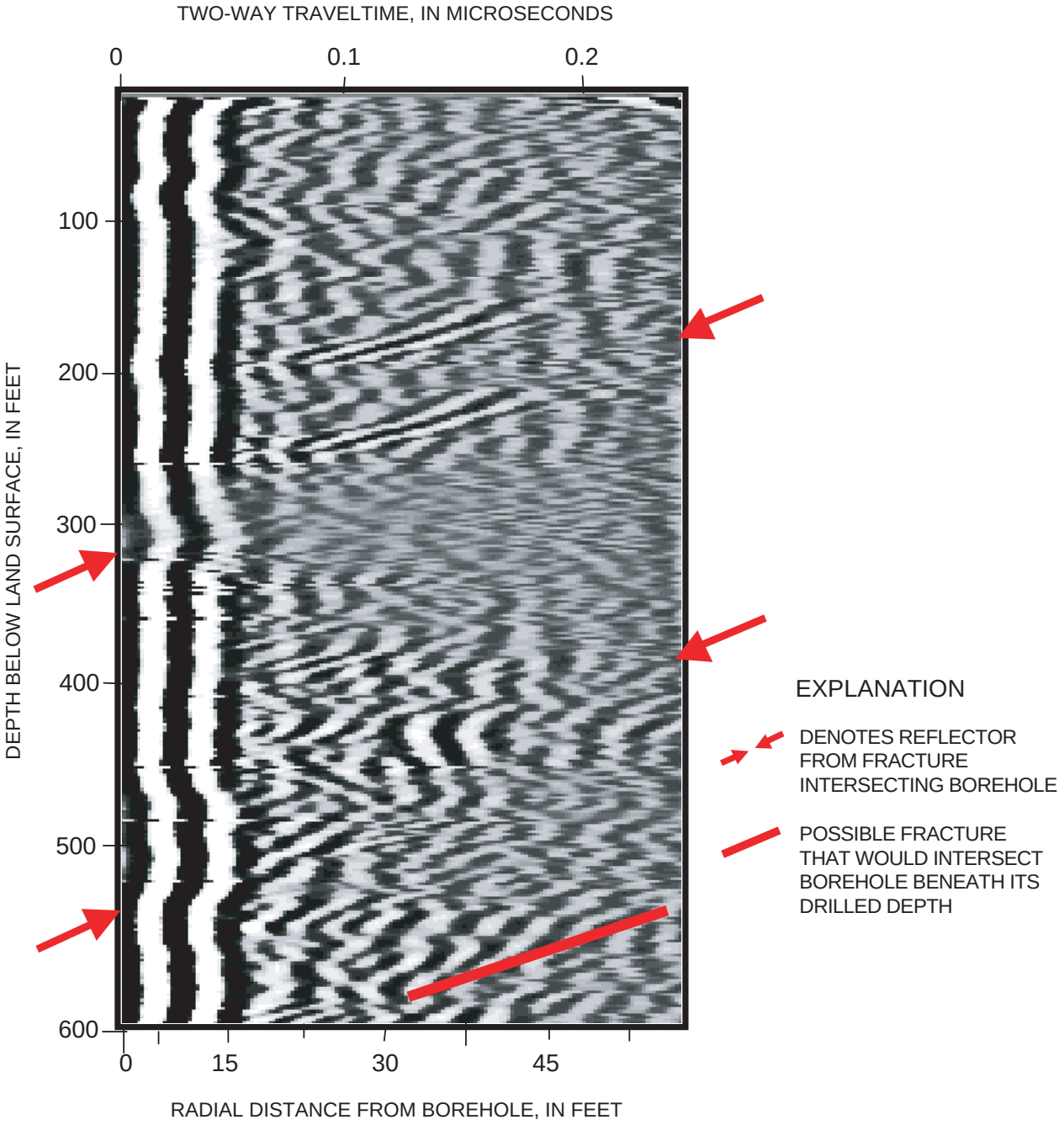

Figure 5. Dipole image of borehole-radar data collected with 60-megahertz antenna from borehole W34ST-B, Manhattan Island, N.Y., 1999. (Borehole location is shown in fig. 1.)

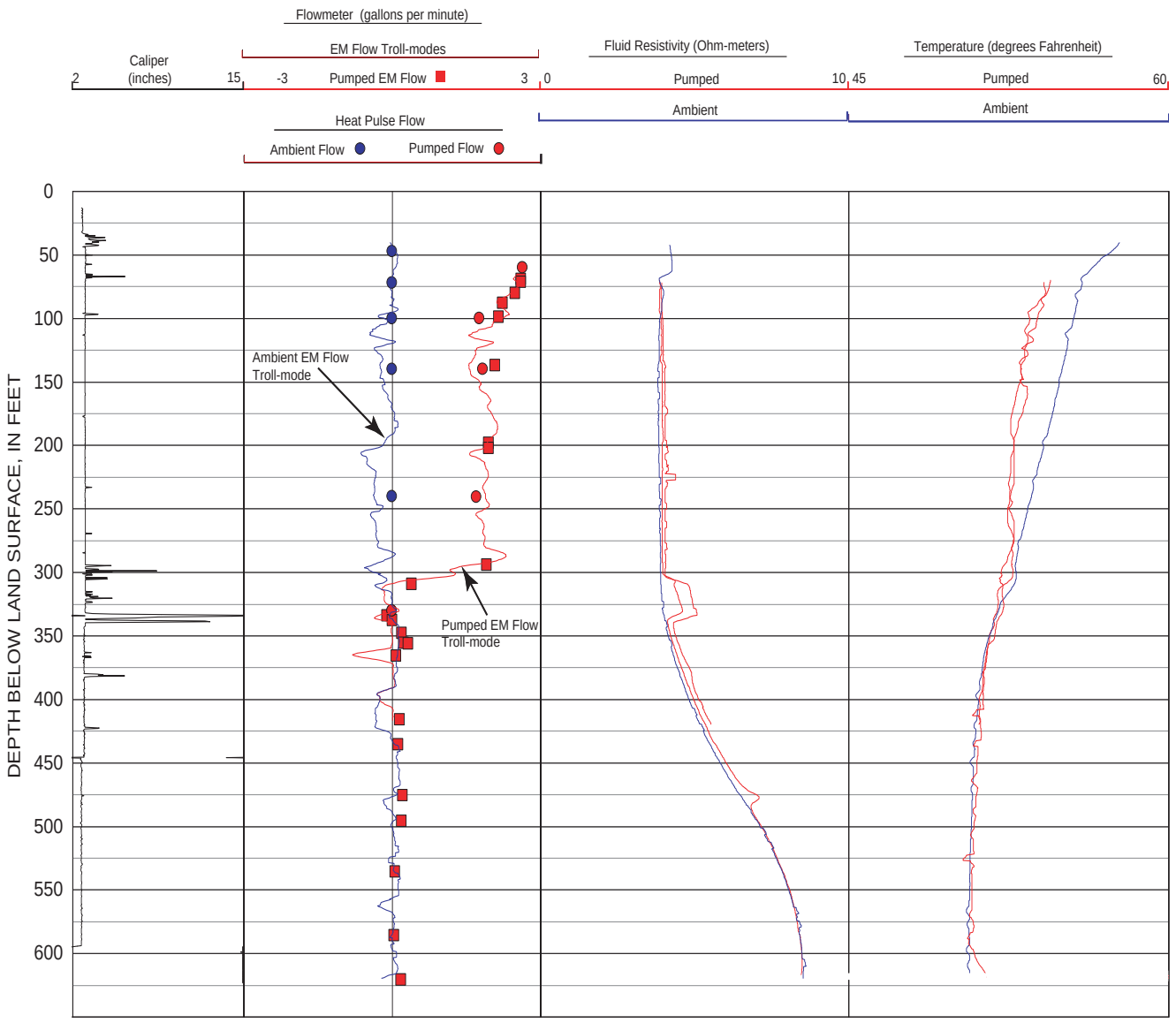

Figure 6. Physical properties of ground-water in borehole W34ST-B, Manhattan Island, N.Y., 1998. (Borehole location is shown in fig. 1.)

azimuths of the three largest fractures within this zone indicate that all have a northeastward dip that may intersect the proposed tunnel within about 220 ft northeast of borehole W34ST-B. The projection of these high-angle features is speculative but is consistent with the absence of such a major feature at borehole W37ST-A, 875 ft to the northeast.

Borehole W37ST-A

Borehole W37ST-A, the second of the three geophysically logged boreholes (fig. 1), extends to a depth of 651.4 ft BLS (-610.09 ft elevation), with steel casing from land surface (41.32 ft elevation) to 15.0 ft BLS (26.32 ft elevation). The bedrock penetrated by the borehole consists of a sequence of gneiss, schistose gneiss, and granite.

Faults, Fractures and Foliation

The ATV and OTV data indicate a total of 254 fractures from below the casing to the bottom of the borehole (see appendix). Large open fractures were detected at 37, 80, 99, 100, 385, and 403 ft BLS (4.32, -38.68, -57.68, -58.68, -343.68 and -361.68 ft elevation). The borehole has a fracture index of 0.40 fracture per foot of borehole. The tadpole plots of fractures (fig. 7) indicate two dense concentrations of fractures at 25 to 150 ft and 350 to 450 ft BLS (16.32 to -108.68 and -308.68 to -408.68 ft elevation). Low-density fracturing is indicated below 500 ft BLS (-458.68 ft elevation). Most small fractures have dip angles less than 45°. No clear pattern of depth and dip azimuths is evident, except that the majority of fractures below 425 ft BLS (-383.68 ft elevation) have dip azimuths toward the northwest (fig. 7). The mean fracture orientation for the 254 fractures is N25°E08°NW (fig. 8). Two fracture-population clusters are indicated in the stereonet plots (fig. 8); one is nearly horizontal; the other dips northwestward. The borehole contains 38 high-angle fractures with dip angles equal to or greater than 70°. Fractures within the proposed TCZ, which extends from 530 ft BLS (-488.68 ft elevation) to the bottom of the borehole, also were analyzed (fig. 8); all fractures from 430 ft BLS (-388.68 ft elevation) to the bottom of the borehole were included to provide a statistically significant sample. Only one small fracture at 624 ft BLS (-582.68 ft elevation) was detected within the proposed TCZ. In all, 20 fractures were used to calculate the mean fracture orientation of N16°E32°NW for the TCZ (fig. 8).

The majority of the foliation tadpoles (fig. 7) dip northwestward with dip angles of 30 to 70°. The mean orientation of total foliation is N06°E55°NW (fig. 8). The TCZ foliation was analyzed from 530 ft BLS (-488.68 ft elevation) to the bottom of the borehole; the mean foliation orientation of the TCZ is N12°E58°NW (fig. 8).

The gamma-log analysis (fig. 7) indicates uniform gamma counts throughout the borehole except at a few isolated locations that correspond to minor mineralogical changes. The SPR and EM logs (fig. 7) show deflections that indicate weathered alteration minerals at four large fracture zones at 80, 100, 385, and 403 ft BLS (-38.68, -58.68, -343.68 and -361.68 ft elevation). The MAG log (fig. 7) indicates low-response zones that correspond to granite intrusions with low magnetite content.

Borehole-deviation analysis of W37ST-A indicates the bottom of the borehole to be a horizontal distance of 21.2 ft from its surface starting point at an azimuth of 118° (fig. 9). The true vertical depth of the borehole is calculated to be 649.51 ft BLS (-608.19 ft elevation).

Borehole radar data indicate two reflectors (possibly fractures) beyond the borehole (and do not intersect the borehole), which had orientations of N16°W32° NE and N04°E43° NE.

Ground-Water Flow Zones

Hydraulic heads in W37ST-A had an average elevation of 13.54 ft. The water levels at this borehole did not appear to be tidally affected. Resolution of the EM flowmeter at this borehole precluded quantitative estimation of the transmissivity of specific fracture zones.

EM flowmeter, fluid-temperature, and fluid-resistivity logs from W37ST-A indicate several transmissive fractures zones (fig. 10). The OTV detected small and medium fractures at 50 to 60 ft BLS (-8.68 to -18.68 ft elevation) with mineral streaks; other possibly transmissive fracture zones at 79 to 83, 98 to 100, 385, and 403 ft BLS (-37.68 to -41.68, -56.68 to -58.68, -343.68 and -361.68 ft elevation) were indicated from the temperature and resistivity logs. Sev-

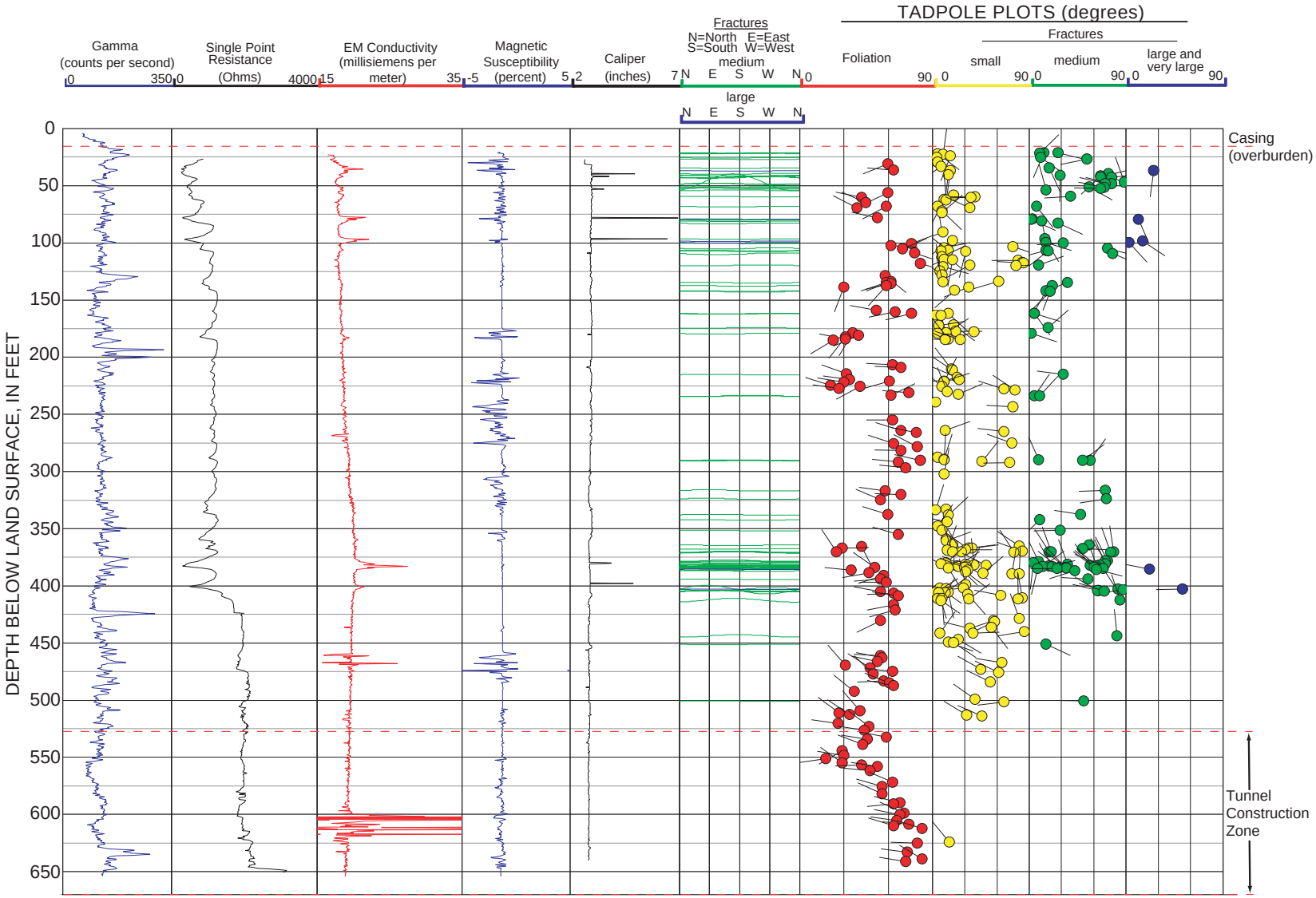

Figure 7. Suite of borehole-geophysical logs from borehole W37ST-A, Manhattan Island, N.Y., 1998. (Borehole location is shown in fig. 1.)

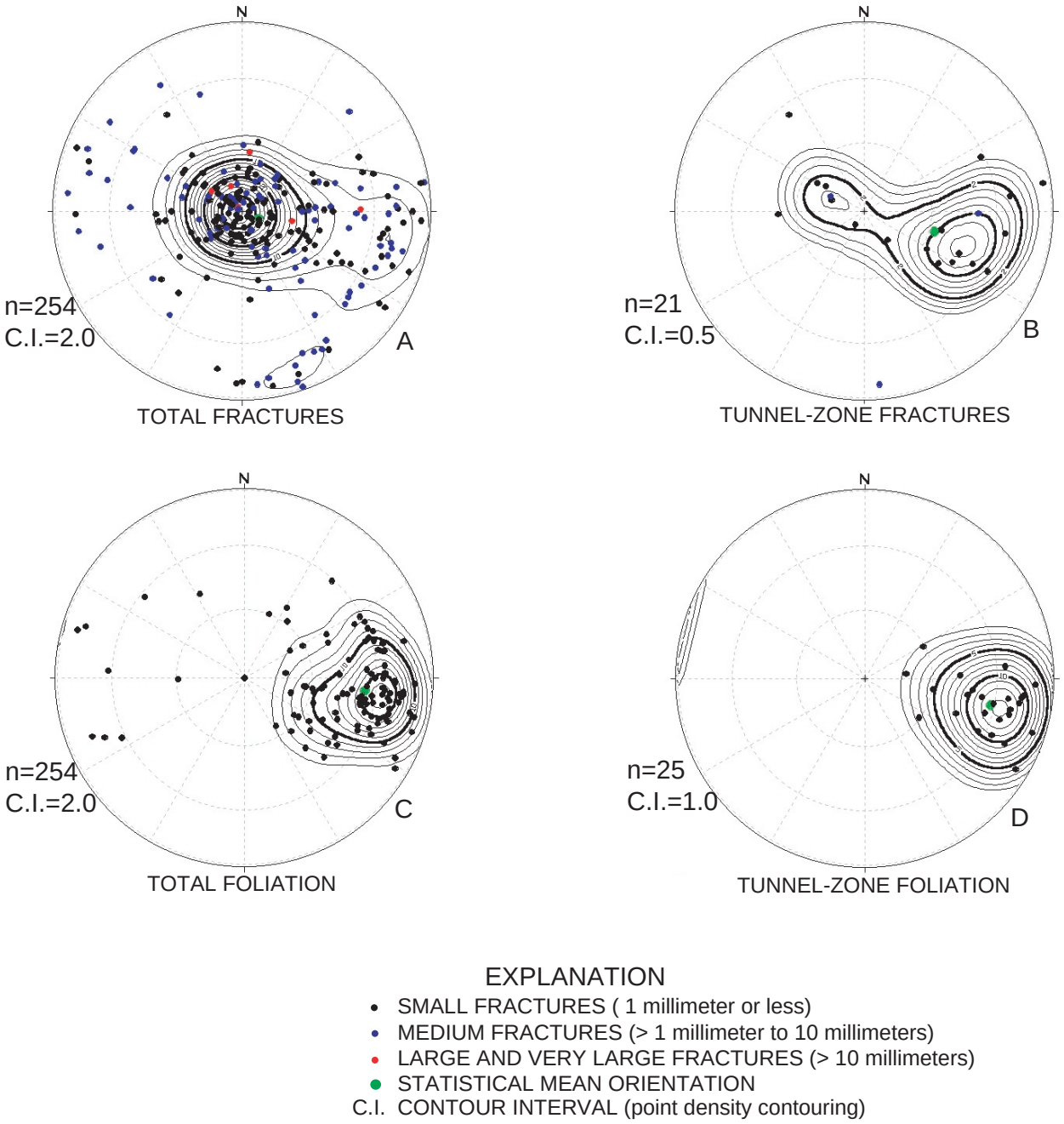

Figure 8. Stereonet plots of borehole W37ST-A, Manhattan Island, N.Y., 1998: A. Total fractures. B. Tunnel-zone fractures. C. Total foliation. D. Tunnel-zone foliation. (Borehole location is shown in fig. 1.)

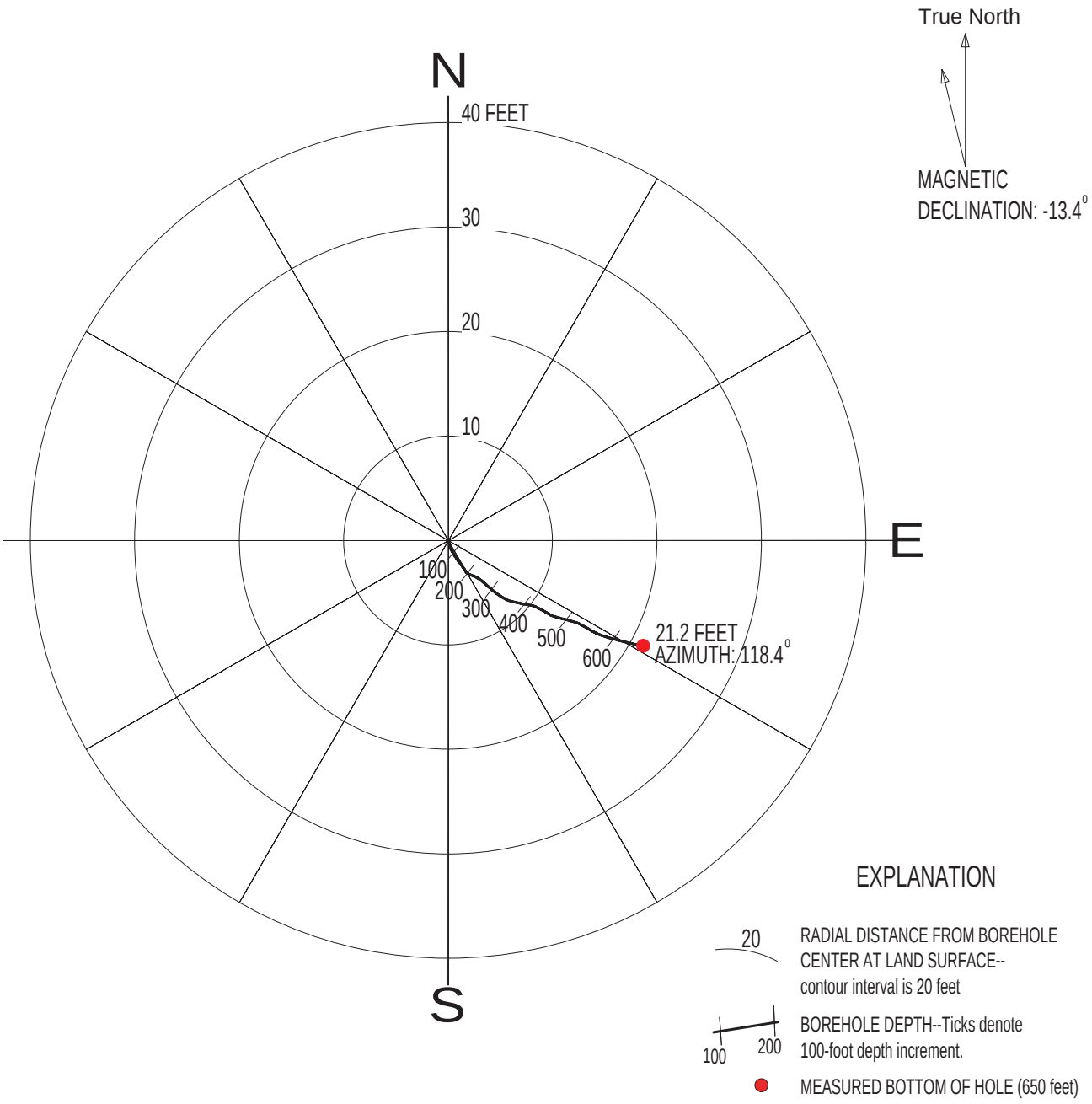

Figure 9. Deviation plot of borehole W37ST-A, Manhattan Island, N.Y., November 1998. (True depth of the borehole is 649.5 feet. Borehole location is shown in fig. 1.)

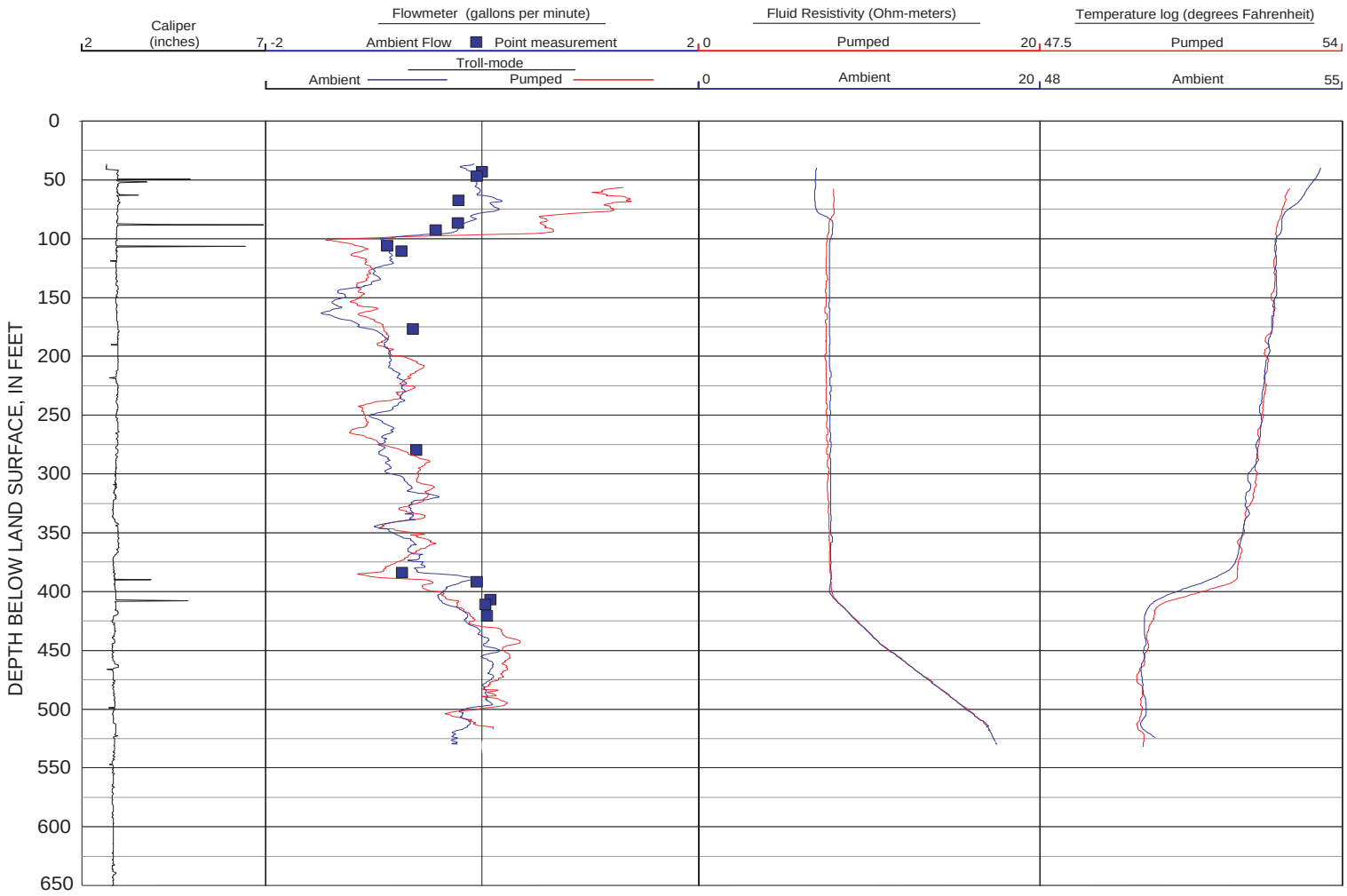

Figure 10. Physical properties of ground water in borehole W37ST-A, Manhattan Island, N.Y., 1998. (Borehole location is shown in fig. 1.)

eral medium fractures and one large fracture were detected by OTV and ATV within the 79- to 83-ft BLS (-37.68- to -41.68-ft elevation) transmissive zone, and two large fractures and several medium fractures were detected within the 98- to 100-ft BLS (-56.68- to -58.68-ft elevation) transmissive fracture zone. The 385- and 403-ft BLS (-343.68- and -361.68-ft elevation) transmissive fracture zones have a large fracture at those depths (fig. 10). EM-flowmeter analysis indicated downward flow from the 50- to 60-ft, 98- to 100-ft, and 385-ft BLS (-8.68- to -18.68-ft, -56.68- to -58.68-ft, and -343.68-ft elevation) zones to the 403-ft BLS (-361.68-ft elevation) zone. The failure of pumping to reverse the direction of flow below the 98- to 100-ft BLS (-56.68- to -58.68-ft elevation) zone indicates significant transmissivity within the 50- to 60-ft, 79- to 83-ft, and 98- to 100-ft BLS (-8.68- to -18.68-ft, -37.68- to -41.68-ft, and -56.68- to -58.68-ft elevation) fracture zones, and relatively low hydraulic head at the 403-ft BLS zone (-361.68-ft elevation, fig. 10).

The borehole was pumped at a rate of 3 gal/min for 1.7 h and produced a drawdown of 2.46 ft, or a specific capacity of 1.22 (gal/min)/ft. Total borehole transmissivity was calculated to be 360 ft^2/d.

Borehole W55ST-A

W55ST-A was the last of three boreholes to be logged within the proposed westside tunnel section (fig. 1). The borehole was drilled to an apparent depth of 619.4 ft BLS (-579.99 ft elevation), with steel casing extending from land surface (39.41 elevation) 34 ft through the unconsolidated sediment overburden to bedrock. The bedrock penetrated by the borehole consists of a sequence of gneiss, schistose gneiss, and granite. A partial collapse of the borehole within bedrock required the installation of steel casing to 150 ft BLS (-110.59 ft elevation) to facilitate geophysical logging. As a result no fracture, foliation, or groundwater data were collected from the top of bedrock at 34 ft BLS (5.41 ft elevation) to the bottom of the inserted casing at 150 ft BLS (-110.59 ft elevation). The poor borehole conditions prevented detection of the microfractures to the extent of the previous two boreholes (W34ST-B and W37ST-A). This borehole, thus is considered undersampled.

Faults, Fractures, and Foliation

The ATV and OTV data (not shown) indicate 126 fractures from the bottom of the inserted casing to the bottom of the borehole (see appendix). Large open fractures were detected at 335, 336, 379, 384, and 605 ft BLS (-295.59, -296.59, -339.59, -344.59, and -565.59 ft elevation). The borehole fracture index of 0.25 fracture per foot of open borehole is the lowest of all three boreholes. The tadpole plots of the fractures (fig. 11) indicate somewhat uniform distributions of fractures with depth. Most small fractures appear to have dip azimuths similar to the foliation. The mean fracture orientation for the 126 fractures is N19°E44°NW (fig. 12). Two fracture-population clusters are indicated in the stereonet plot (fig. 12); one is nearly horizontal and dipping slightly to the east; the second dips northwestward (fig. 12). The borehole contains 12 high-angle fractures throughout the borehole with dip angles equal to or exceeding 70°. Fractures within the proposed TCZ from 462 ft BLS (-422.59 ft elevation) to the bottom of the borehole were included to provide a statistically significant sample. In all, 43 fractures (13 of which are medium to large) were detected within the proposed TCZ and have a mean fracture orientation of N13°E51°NW (fig. 12).

The foliation tadpoles (fig. 11) indicate nearly constant dip angles of about 60° with azimuths toward the northwest. The mean orientation of foliation for the entire borehole is N16°E 60°NW; and that for the TCZ is N20°E 61°NW (fig. 12).

The gamma-log (fig. 11) analysis indicates uniform gamma counts throughout most of the borehole except at isolated locations. The SPR log (fig. 11) has conductive spikes, some that correspond to fractures at 226 to 231 and 475 ft BLS (-186.59 to -191.59 and -435.59 ft elevation). The EM log (fig. 11) has a muted response, similar to the SPR log. The bedrock seems to increase in resistance with depth. The MAG log (fig. 11) shows a clear contact at 375 ft BLS (-335.59 ft elevation) that indicates a probable lithologic change to magnetite-poor rock.

Borehole-deviation analysis of W55ST-A (fig. 13) indicates the bottom of the borehole to be a horizontal distance of 28.9 ft from its surface starting point at an azimuth of 82°. The true vertical depth of the borehole is estimated to be 618.2 ft BLS (-578.79 ft elevation, fig. 13).

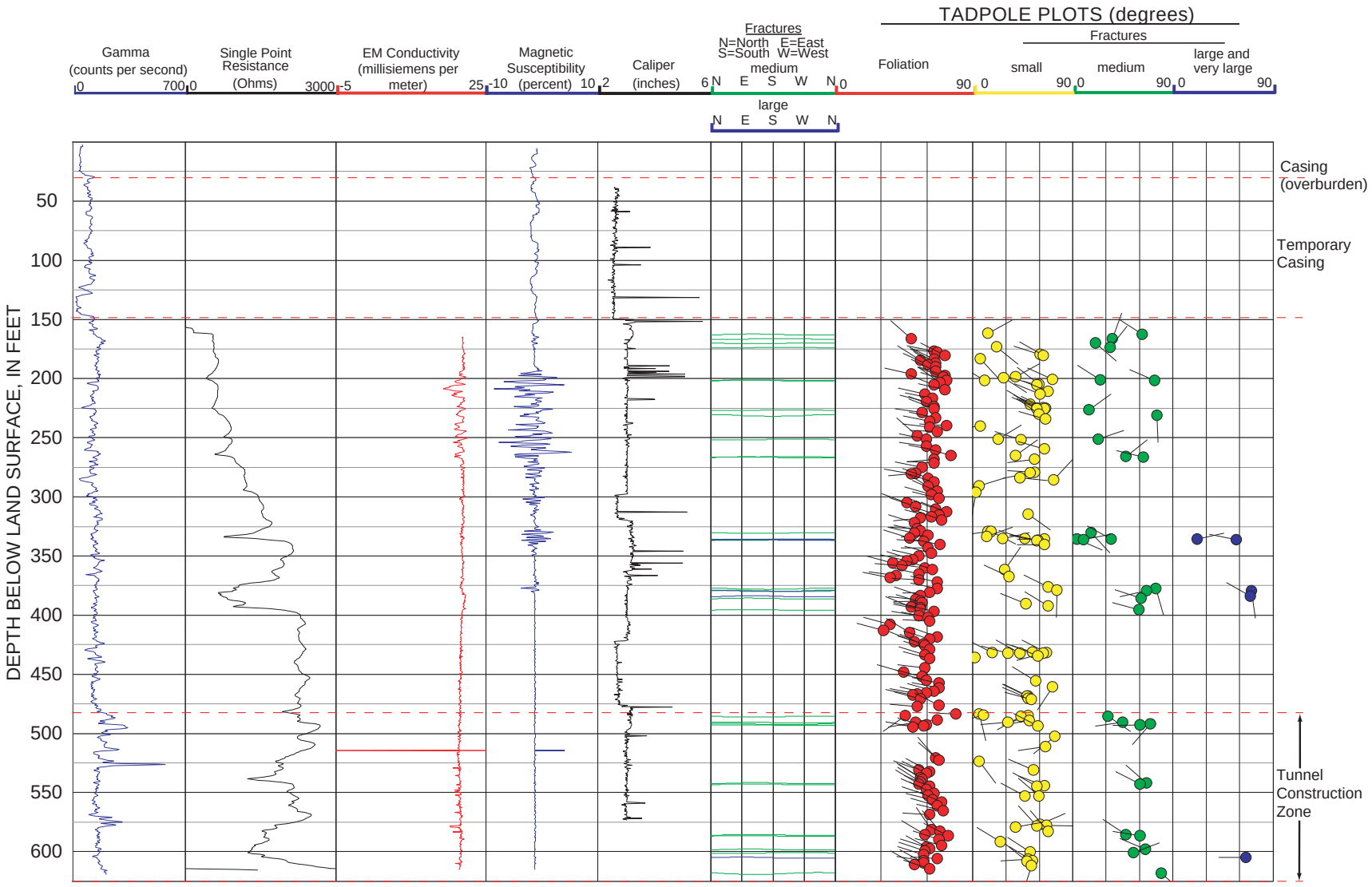

Figure 11. Suite of borehole-geophysical logs from borehole W55ST-A, Manhattan Island, N.Y., 1998. (Borehole location is shown in fig. 1.)

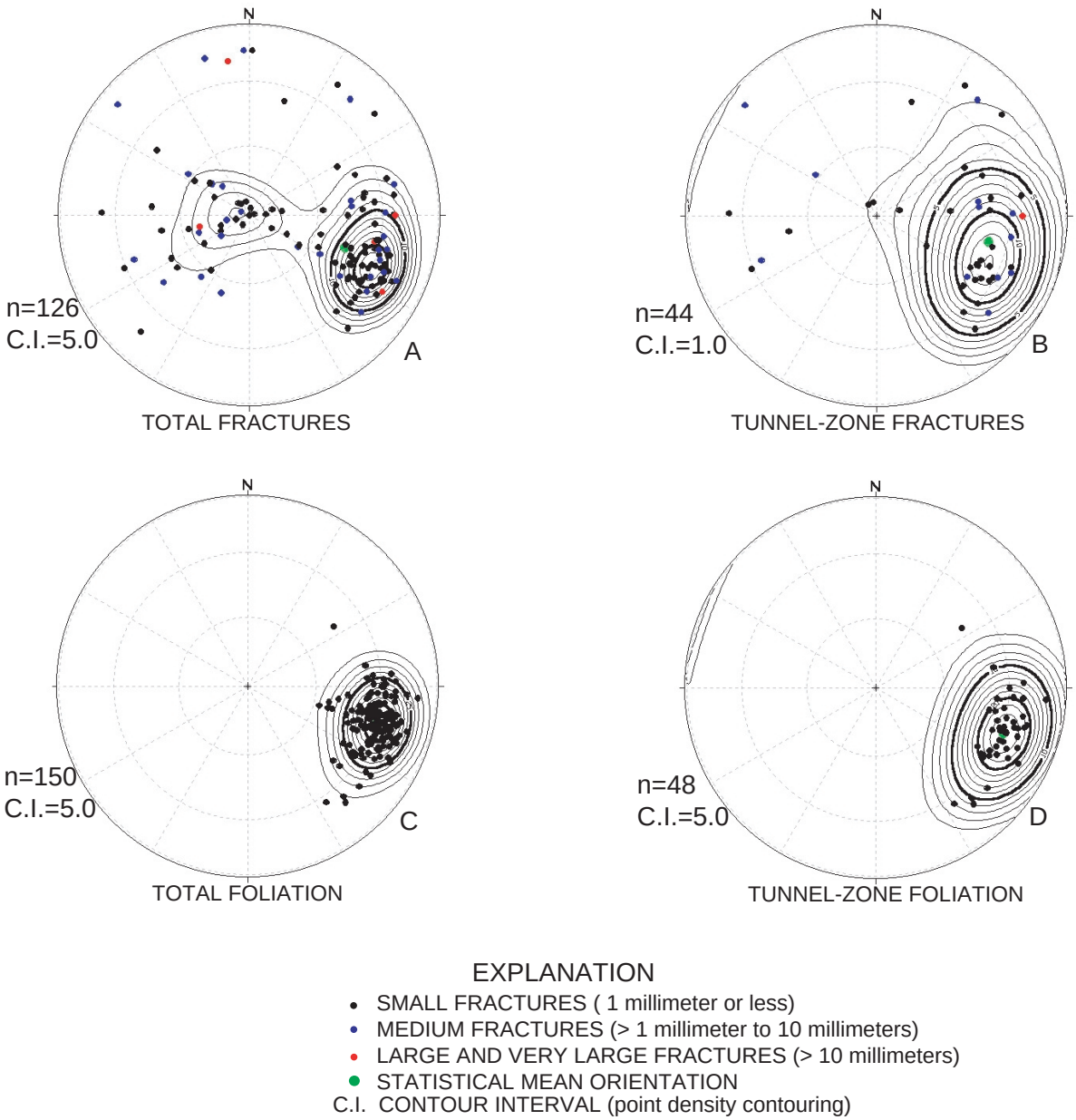

Figure 12. Stereonet plots of borehole W55ST-A, Manhattan Island, N.Y., 1998: A. Total fractures. B. Tunnel-zone fractures. C. Total foliation. D. Tunnel-zone foliation. (Borehole location is shown in fig. 1.)

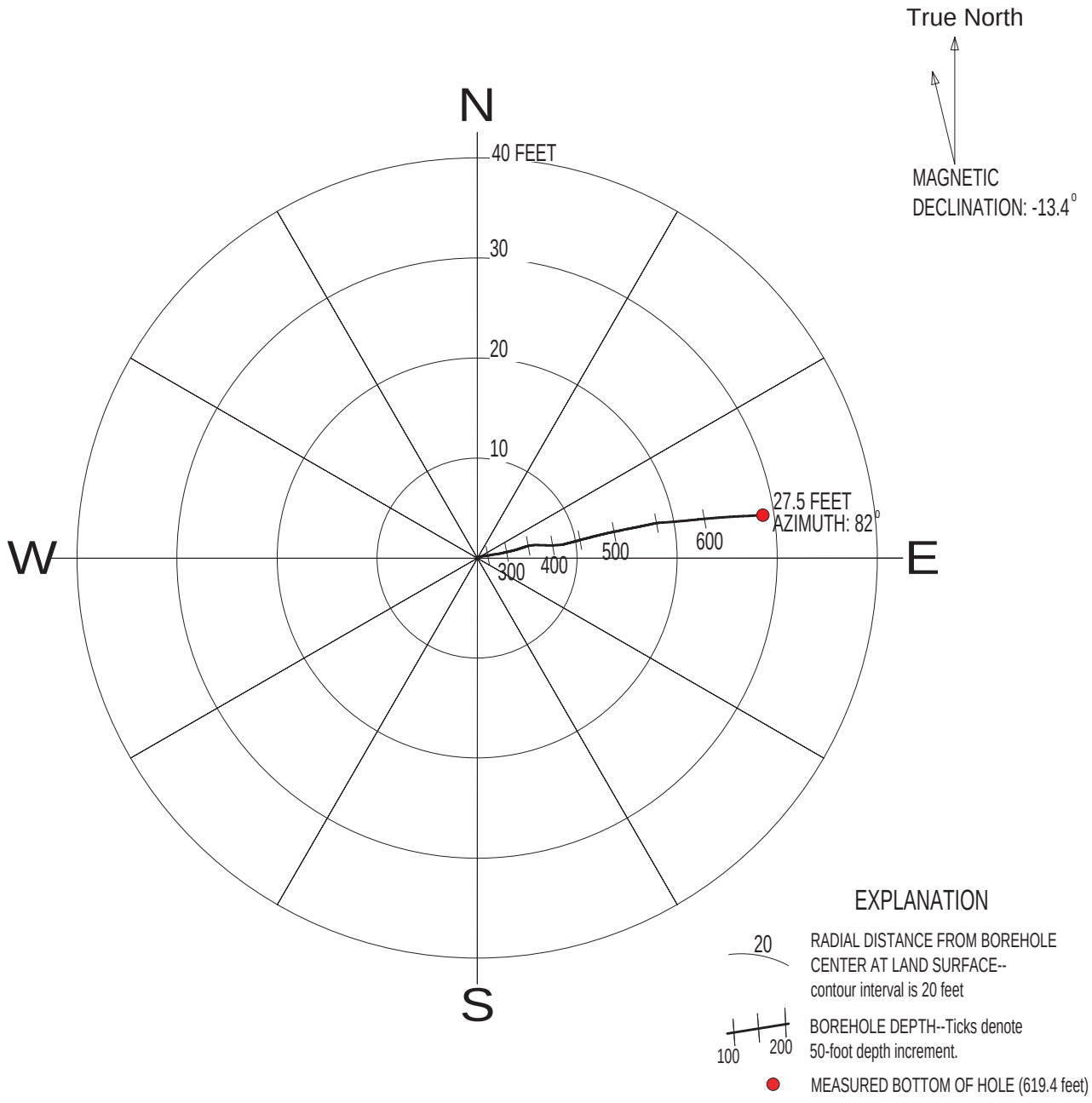

Figure 13. Deviation plot of borehole W55ST-A, Manhattan Island, N.Y., November 1998. (True depth of the borehole is 618.2 feet. Borehole location is shown in fig. 1.)

Borehole radar data indicate four reflectors (possibly fractures) beyond the borehole with orientations of N24°E59°SE, N44°E56°SE, N03°W50°NE, and N64°E53°SE.

Ground-Water Flow Zones

Hydraulic heads in W55ST-A had a mean elevation of 29.13 ft and appeared to be tidally affected. Equipment malfunctions and poor borehole conditions hampered the ability to calculate transmissivity of some fracture zones.

Heat-pulse flowmeter and fluid-resistivity logs indicate transmissive fracture zones at 162 to 170, 226 to 231, and 330 to 619.4 ft BLS (-122.59 to -130.59, -186.59 to -191.59, and -290.59 to -611.29 ft elevation, fig. 14). Three medium fractures at the 162- to 170-ft BLS (-122.59- to -130.59-ft elevation) fracture zone indicate no detectable ambient flow but significant upflow and transmissivity during pumping. The fluid-resistivity log indicates a deflection or slope change at the 226- to 231-ft BLS (-186.59 to -191.59, ft elevation) fracture zone, and the heat-pulse flowmeter indicates no detectable ambient flow and only minor upflow during pumping. The limited measurements from the 330- to 619.4-ft BLS (-290.59- to -611.29-ft elevation, bottom of borehole) fracture zone precluded calculation of specific fracture transmissivity values or hydraulic head. The fluid-resistivity log indicates a deflection or change in slope at 342 to 380 ft BLS (-302.59 to -340.59 ft elevation, fig. 14).

Pumping at a rate of 1.1 gal/min for 1.9 hours produced a drawdown of 24.2 ft, or a specific capacity of 0.05 (gal/min)/ft. Total borehole transmissivity was calculated to be 11 ft^2/d. Analysis of the ambient and pumping conditions indicated three transmissive zones at 162 to 170 ft, 226 to 231 ft, and 330 to 619.4 ft BLS (-122.59 to -130.59 ft, -186.59 to -191.59 ft, and -290.59 to -611.29 ft elevation), with estimated transmissivities of 5.6, 0.3, and 5.1 ft^2/d, respectively. Thus, 46 percent of the ground water was produced from the 330- to 619.4-ft BLS fracture zone (-290.59- to -611.29-ft elevation, bottom of borehole) .

SUMMARY AND CONCLUSIONS

In 1970, the New York City Department of Environmental Protection (NYCDEP) began construction of a third tunnel to supply water to New York City in case that one of the two present tunnels should require repair. In 1998, the U.S. Geological Survey (USGS), in cooperation with the NYCDEP, began a study to apply advanced borehole-geophysical methods to assess crystalline bedrock in southeastern New York. Three boreholes on western Manhattan Island were drilled by the NYCDEP to provide cores, geophysical logs, and geotechnical information for the design and construction of City Water Tunnel 3. Two additional boreholes (GroveST-A, and W26ST-A) were drilled and only fracture and foliation orientations were measured. The geophysical logs provided data on the deviation of the boreholes from vertical, the location and orientation (dip azimuth and dip) of fractures (OTV and ATV), the orientation (dip azimuth and dip) of rock foliation (OTV), locations of contacts between rock units of differing types, and locations of transmissive (water-producing) fractures; they also provided information on the rocks' magnetic susceptibility, electrical resistivity and resistance, the direction and quantity of ground-water flow within the borehole, resistance and temperature of ground water, a profile of the borehole diameter, and the extent of fractures or geologic features up to 100 ft beyond the borehole.

The bedrock contains numerous fractures that intersect the study area. Depth to bedrock ranges from 8 to 34 ft BLS. Overlying the bedrock are unconsolidated sediments that were cased off with steel in wells completed in the three boreholes. Small fractures had apertures of 0.04 in. (1 mm) or less, medium fractures had apertures of >0.04 to 0.39 in. (>1 to 10 mm), large fractures had apertures >0.39 in. (>10 mm) and very large fractures had apertures >9.8 in. (>25 cm). The tunnel construction zone was defined as a horizon ranging from 50 ft above the roof to 50 ft below the floor of the proposed tunnel; this represents the major area of proposed construction in the interval from 540 to 625.7 ft BLS (-499.73 to -585.43 ft elevation) at W34ST-B, 530 to 651.4 ft BLS (-488.68 to -610.09 ft elevation) at W37ST-A, and 462 to 619.4 ft BLS (-422.59 to -579.99 ft elevation) at W55ST-A. Equal-area nets and tadpole analyses were used to identify foliation and fracture relations. (Tadpoles are circles with tails plotted with respect to a horizontal scale to indicate the degree of dip-plunge angle of the structures from 0 to 90°. The tail of each tadpole points to the dip azimuth of the structure.)

Three-dimensional analysis of the medium and large fractures associated with the 328-330 ft BLS (-287.73 to -289.73 ft elevation) fracture zone in

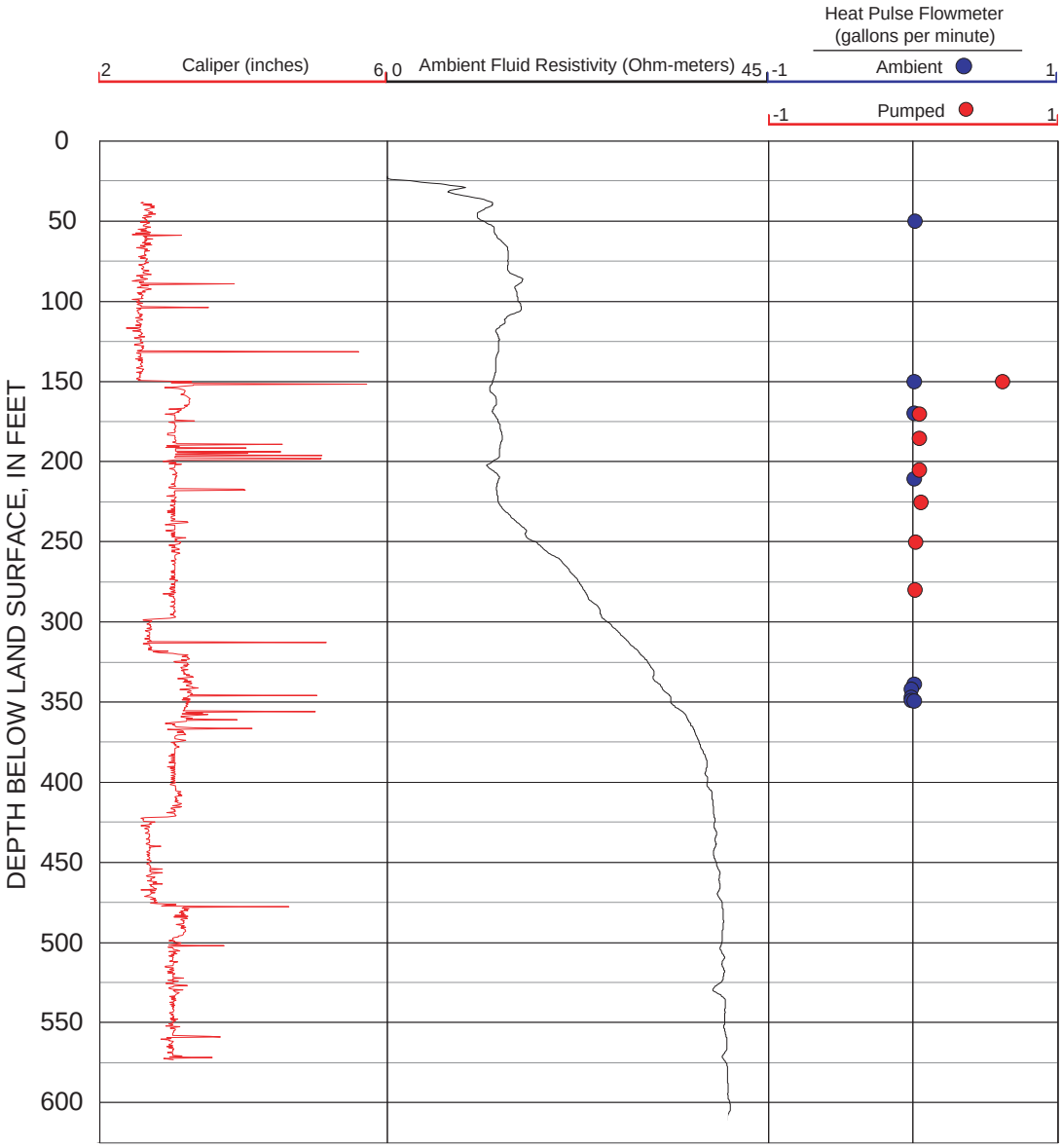

Figure 14. Physical properties of ground-water in borehole W55ST-A, Manhattan Island, N.Y., 1998. (Borehole location is shown in fig. 1.)

W34ST-B indicates that these highly transmissive fractures may intersect the proposed tunnel to within a distance of 220 ft northeast of the borehole. These fractures may produce appreciable quantities of ground-water flow into the tunnel and could thereby affect construction. Fracture indexes range from 0.25 to 0.44 fracture per foot of bedrock. No correlation is indicated between fracture orientation and depth. Total-borehole fracture populations are either nearly horizontal or moderate- to high-angle dip with a northwest azimuth. The intersection of these fracture populations could result in block- or wedge-failure during tunnel construction. Foliation analysis indicates some relation between depth and foliation. Overall, the average foliation of the bedrock ranges from southwest to northwest dip azimuth. Foliation dip azimuths within the Tunnel Construction Zone range from southwest to northwest, with dip angles ranging from 58° to 65°.

Analysis of the 60-Mhz directional radar indicates strong radar reflectors, which probably are fractures that extend beyond the boreholes and probably would intersect the boreholes if the boreholes were deeper. Radar analysis indicates that some of these fractures, if water bearing, could produce appreciable quantities of ground-water flow into the tunnel and could thereby affect construction.

Water levels in the fractured bedrock ranged from 29.1 ft elevation in the northern part of the study area (W55ST-A) to 10.5 ft elevation in the southern part (W34ST-B). Transmissivity values for most transmissive fracture zones in each borehole were estimated, if possible. Transmissive fracture zones were delineated by correlating inflow zones interpreted from heat-pulse flowmeter logs with major fracture zones indicated by other geophysical logs. Each of the three boreholes tested had several transmissive fracture zones. Some of these fractures had high transmissivity, especially at those boreholes with moderate to high total borehole transmissivity.

REFERENCES CITED

Baskerville, C.A., 1992, Bedrock and engineering geologic maps of Bronx County and parts of New York and Queens Counties, New York: U.S. Geological Survey Miscellaneous Investigations Series, map I-2003, 2 sheets, scale 1:24,000.

Bradbury, K.R., and Rothschild, E.R., 1985, A computerized technique for estimating the hydraulic conductivity of aquifers from specific-capacity data; Groundwater, v. 23, no. 2, p. 240-246.

Keys, W.S., and MacCary, L.M., 1971, Application of borehole geophysics to water-resources investigations: U.S. Geological Survey Techniques of Water Resources Investigations, book 2, chap. E1, 126 p.

Keys, W.S.,1990, Borehole geophysics applied to water-resources investigations: U.S. Geological Survey Techniques of Water Resources Investigations, book 2, chap. E2, 150 p.

McNeill, J.D, Hunter, J.A., and Bosner, M., 1996, Application of a borehole induction magnetic susceptibility logger to shallow lithological mapping: Journal of Environmental and Engineering Geophysics, v. 0, no. 2, p. 77-90.

Molz, F.J., Morin, R.H., Hess, A.E., Melville, J.G., and Guven, Oktay, 1989, The impeller meter for measuring aquifer permeability variations—evaluation and comparison with other tests: Water Resources Research, v. 25, no. 7, p. 1677-1683.

Paillet, F. L., 1998, Flow modeling and permeability estimation using borehole flow logs in heterogeneous fractured formations: Water Resources Research, v. 34, no. 5, p. 997-1010.

Paillet, F. L., 2000, A field technique for estimating aquifer parameters using flow log data: Ground Water, v. 38, no. 4, p. 510-521.

Serra, Oberto, 1984, Fundamentals of well-log interpretation: New York, Elsevier, 423 p.

Singha, Kamini, Kimball, Kari, and Lane, J.W., Jr., 2000, Borehole-Radar Methods-Tools for characterization of fractured rock: U.S. Geological Survey Fact Sheet 054-00, 4 p.

Stumm, F., Paillet, F., Williams, J.H., and Lane, J.W., 2000, Geohydrologic assessment of crystalline bedrock for the New York City Water-Tunnel Project by use of advanced borehole-geophysical methods, *in* Proceedings of the Seventh International Symposium on Borehole Geophysics for Minerals, Geotechnical, and Groundwater Applications, October 24-26, 2000, Denver, Colorado, Minerals and Geotechnical Logging Society, p. 19-27.

Williams, J.H., and Conger, R.W., 1990, Preliminary delineation of contaminated water-bearing fractures intersected by open-hole bedrock wells: Groundwater Monitoring and Review, v. 10, no. 4, p. 118-126.

Williams, J.H., and Johnson, C.D., 2000, Borehole-wall imaging with acoustic and optical televiewers for fractured-bedrock aquifer investigations, *in* Proceedings of the Seventh International Symposium on Borehole Geophysics for Minerals, Geotechnical, and Groundwater Applications, October 24-26, 2000, Denver, Colorado, Minerals and Geotechnical Logging Society, p. 43-53.

Appendix. Depth, dip azimuth, and dip angle of fractures and foliation observed by optical televiewer in five boreholes (W34ST-B, W37ST-A, W55ST-A, W26ST-A, and GroveST-A), Manhattan Island, N.Y., 2000-01

[Depths are in feet below land surface. SM, small fracture (0.04 inch or less); MED, medium fracture (greater than 0.04 to 0.39 inch); LG, large fracture (greater than 0.39 in to 9.8 inches); VLG, very large fracture (greater than 9.8 inches); GW, ground water, FLT, fault. Borehole locations are shown in fig. 1.].

Depth	Dip azimith, in degrees	Dip angle, in degrees	Fracture size
W34ST-B			
Fractures			
15.5	223	45	MED
15.6	274	23	MED
15.6	290	21	MED
15.8	235	48	LG
24.6	280	11	LG
24.7	121	6	LG
24.8	211	16	SM
30.8	222	4	LG
35.1	247	33	SM
35.3	246	45	MED
37.2	247	60	SM
40.1	99	35	SM
41.0	277	28	SM
41.1	164	84	SM
41.6	276	55	MED
41.7	262	51	SM
43.4	269	28	MED
43.6	290	30	SM
44.2	240	44	SM
47.3	222	11	MED
48.9	121	37	SM
49.7	238	56	SM
51.0	280	19	MED
51.2	218	30	MED
52.0	12	6	SM
52.0	256	9	MED
54.1	246	24	MED
54.4	261	17	MED
55.9	264	17	SM
58.4	255	65	SM
59.4	216	20	SM
60.0	217	16	LG
60.7	264	38	SM
61.7	247	53	SM
62.2	250	18	MED
63.7	186	9	SM
63.9	226	5	SM
65.2	241	20	SM
65.3	238	21	SM
65.8	238	15	SM
67.4	216	6	SM
67.6	311	13	SM
68.7	257	15	MED
69.9	304	9	SM
70.5	253	53	SM
70.6	247	51	SM
72.1	35	6	MED GW
72.2	64	12	MED GW
73.1	281	9	SM
73.4	304	13	SM
73.7	294	22	SM
75.9	267	11	SM
76.6	251	32	SM
77.0	279	6	MED GW
77.1	282	16	MED GW
77.9	62	3	SM
78.0	259	52	SM
78.4	197	9	SM
80.1	222	18	MED
81.0	265	52	SM
82.7	43	19	MED
82.8	52	5	SM
85.8	287	18	SM
86.3	286	26	SM
87.5	298	25	SM
88.4	92	30	SM
89.0	75	29	SM
89.2	282	16	MED GW
89.3	1	22	MED GW
89.6	327	10	MED
89.7	130	7	SM
90.0	45	12	LG GW
90.5	19	26	MED
91.7	135	2	SM
95.2	306	32	SM
100.7	292	37	SM
103.9	278	18	MED
104.4	95	8	MED GW
104.5	47	9	SM
106.8	281	18	SM
112.9	300	5	SM
115.6	127	11	SM
117.7	273	43	SM
118.2	271	31	SM

Appendix. Depth, dip azimuth, and dip angle of fractures and foliation observed by optical televiewer in five boreholes (W34ST-B, W37ST-A, W55ST-A, W26ST-A, and GroveST-A), Manhattan Island, N.Y., 2000-01--continued

Depth	Dip azimith, in degrees	Dip angle, in degrees	Fracture size
120.7	213	63	SM
121.1	272	50	SM
121.7	262	37	SM
121.9	278	32	SM
123.0	282	18	SM
124.2	256	58	SM
125.5	272	67	SM
127.5	16	18	MED
127.5	136	4	MED GW
128.2	22	12	MED
128.3	93	20	MED GW
130.2	250	56	SM
141.1	37	16	MED GW
142.5	302	18	SM
165.2	257	55	SM
165.3	256	57	SM
165.8	263	41	SM
167.2	250	12	MED
167.9	65	17	SM
169.5	182	72	SM
176.9	144	15	SM
177.0	130	12	SM
177.6	31	45	MED
181.8	250	54	SM
182.2	283	50	MED
186.3	71	24	SM
191.9	307	82	MED
192.2	299	89	MED
193.4	271	75	MED
204.3	273	30	SM
224.7	165	71	SM
226.1	300	73	MED
227.8	112	75	MED
230.6	77	24	SM
230.6	82	14	SM
263.7	101	23	SM
264.0	131	23	MED
266.7	241	34	SM
270.0	232	57	MED
271.5	222	60	SM
273.2	223	77	MED
276.2	28	16	SM
278.6	201	78	MED
281.8	267	25	MED
284.3	228	65	MED
286.2	214	77	MED
289.2	314	9	MED
289.3	15	15	LG
289.4	212	61	LG
289.5	20	25	MED
290.1	55	30	MED
290.4	75	29	MED
290.8	45	25	SM
290.9	49	19	SM
291.0	213	62	SM
292.2	7	9	MED
292.3	222	70	LG
292.3	38	20	MED
292.3	37	19	MED
292.8	67	34	MED
293.1	38	20	LG
293.3	74	34	LG
293.5	39	39	VLG
293.8	320	7	SM
294.3	66	13	SM
294.4	283	4	LG
294.5	133	3	LG
295.3	45	26	LG
295.4	59	26	MED
295.6	37	26	SM
296.5	357	82	SM
297.0	237	3	MED
297.0	114	19	MED
297.1	77	18	MED
297.7	294	5	SM
297.8	133	12	SM
297.9	71	16	MED
298.1	340	73	MED
298.2	346	71	MED
298.9	69	26	LG
299.7	63	8	LG
299.9	31	20	MED
300.1	56	16	SM
300.3	32	9	SM
309.9	327	37	SM
310.1	319	45	SM
311.3	291	8	SM
312.4	291	75	MED

Appendix. Depth, dip azimuth, and dip angle of fractures and foliation observed by optical televiewer in five boreholes (W34ST-B, W37ST-A, W55ST-A, W26ST-A, and GroveST-A), Manhattan Island, N.Y., 2000-01--continued

Depth	Dip azimith, in degrees	Dip angle, in degrees	Fracture size
312.6	283	46	MED
312.8	274	41	MED
314.0	309	87	MED
315.0	279	33	MED
315.2	316	42	MED
316.1	293	51	MED
317.5	133	32	SM
318.0	268	82	SM
318.5	161	12	SM
320.5	347	20	SM
320.7	343	32	SM
321.9	2	35	MED
322.6	100	73	MED
324.5	243	77	MED
326.4	259	47	SM
327.0	270	51	SM
327.5	301	36	SM
327.6	314	13	MED
328.5	47	52	LG
328.9	353	69	VLG
329.5	346	69	VLG
330.0	359	49	LG
330.2	348	34	MED
330.5	168	33	MED
330.6	341	37	MED
330.8	14	32	MED
330.9	1	36	MED
331.2	339	44	MED
331.7	353	49	MED
332.0	333	43	MED
332.2	358	43	MED
332.9	344	68	VLG
334.0	304	32	MED
334.3	315	18	MED
335.5	341	21	SM
335.6	272	26	MED
335.7	312	47	MED
336.1	294	45	MED
336.3	322	22	SM
336.9	297	78	MED
337.3	327	34	MED
339.0	341	78	SM
339.4	318	70	SM
340.0	253	59	SM
340.9	287	34	MED
341.6	264	44	MED
342.0	285	37	MED
342.7	273	27	SM
343.4	287	38	SM
344.7	295	20	SM
345.6	317	9	SM
346.0	276	27	MED
346.4	237	68	SM
347.9	272	30	SM
348.1	281	9	SM
348.3	242	67	SM
349.3	315	24	SM
349.5	303	32	SM
354.6	233	76	MED
356.8	225	73	MED
357.6	50	82	MED
360.7	42	79	MED
362.8	281	55	MED
362.9	302	33	MED
363.0	294	23	SM
363.2	271	34	SM
364.2	44	77	SM
366.0	33	71	MED
366.5	292	67	SM
366.6	21	67	SM
366.8	299	22	SM
367.1	271	75	MED
368.0	277	74	MED
368.7	307	31	SM
369.0	41	78	MED
370.8	251	25	SM
371.4	311	14	SM
373.9	299	22	MED
374.1	290	38	MED
374.4	296	73	MED
378.1	335	80	MED
379.3	335	80	MED
380.5	148	89	MED
383.2	145	87	MED
396.9	345	41	SM
397.9	237	47	MED
446.6	304	73	MED
470.8	284	50	MED

Appendix. Depth, dip azimuth, and dip angle of fractures and foliation observed by optical televiewer in five boreholes (W34ST-B, W37ST-A, W55ST-A, W26ST-A, and GroveST-A), Manhattan Island, N.Y., 2000-01--continued

Depth	Dip azimith, in degrees	Dip angle, in degrees	Fracture size
471.3	286	32	SM
473.5	273	43	SM
481.3	359	88	SM
484.6	0	20	SM
494.1	297	25	SM
500.8	23	17	SM
519.1	274	28	SM
531.6	304	59	MED
540.9	300	4	MED
541.5	257	88	MED
544.0	101	39	MED
Foliation			
41.8	256	46	
44.0	251	48	
44.8	267	46	
53.6	244	63	
54.2	269	57	
57.0	268	70	
61.3	255	76	
64.0	245	70	
70.6	249	63	
81.6	272	34	
92.6	270	60	
95.0	306	43	
97.0	242	69	
102.0	262	77	
113.1	255	47	
114.6	231	54	
116.2	265	55	
120.8	253	62	
122.0	254	62	
124.6	264	61	
129.2	246	64	
130.1	249	65	
131.9	242	58	
132.4	236	55	
133.9	243	62	
135.5	248	64	
141.5	259	67	
163.1	253	65	
165.2	262	55	
165.8	252	40	
167.3	252	62	
168.3	276	68	
170.0	258	63	
172.1	259	38	
174.4	269	51	
177.7	262	53	
178.6	272	65	
180.2	268	55	
182.9	281	74	
183.8	282	75	
188.1	255	61	
207.5	248	48	
209.2	245	45	
210.5	252	57	
220.2	252	62	
226.3	251	51	
237.6	246	59	
245.4	257	44	
246.3	302	52	
247.3	249	44	
253.2	245	54	
256.5	252	58	
260.4	254	52	
261.6	252	59	
263.2	248	55	
263.8	248	40	
264.6	254	38	
265.4	253	46	
266.8	239	55	
275.5	272	61	
279.3	273	43	
283.6	290	63	
302.4	240	48	
308.4	359	70	
309.4	330	67	
311.3	308	49	
313.9	306	41	
314.8	284	52	
316.2	288	38	
316.9	305	42	
317.6	277	48	
318.2	307	31	
345.5	311	32	
346.0	268	25	
351.3	66	65	
352.4	93	57	

Appendix. Depth, dip azimuth, and dip angle of fractures and foliation observed by optical televiewer in five boreholes (W34ST-B, W37ST-A, W55ST-A, W26ST-A, and GroveST-A), Manhattan Island, N.Y., 2000-01--continued

Depth	Dip azimith, in degrees	Dip angle, in degrees	Fracture size
380.1	316	66	
396.2	28	61	
397.1	11	53	
399.6	45	45	
403.4	260	71	
407.2	288	70	
412.6	60	35	
412.9	92	44	
413.4	81	31	
414.9	121	36	
417.1	256	74	
419.1	244	69	
421.3	254	70	
422.2	240	67	
423.6	248	56	
430.7	259	70	
431.9	295	65	
440.6	246	38	
441.1	262	52	
448.7	304	52	
455.2	270	39	
467.4	221	54	
469.1	251	38	
484.0	268	68	
487.0	270	67	
487.8	274	67	
490.6	115	86	
492.6	311	88	
506.5	278	67	
508.8	260	71	
515.7	298	77	
516.5	291	81	
522.4	261	64	
525.2	255	71	
528.8	267	64	
531.6	294	66	
547.4	300	60	
548.9	221	58	
550.2	212	61	
551.4	221	63	
553.0	203	54	
556.9	235	61	
570.5	245	54	
572.9	250	75	
588.7	250	64	
591.8	257	66	
617.1	238	69	
617.6	262	65	
618.7	274	60	
W37ST-A			
Fractures			
20.9	203	14	MED
21.3	103	27	MED
21.4	46	10	MED GW
22.0	126	5	SM
22.7	15	19	SM
22.7	8	10	SM
24.1	200	17	SM
25.2	125	11	MED
25.4	234	4	SM
26.5	259	54	MED
29.5	234	5	SM GW
33.3	235	8	SM GW
34.3	155	19	MED GW
36.8	188	17	SM
36.9	187	26	LG
39.5	120	56	MED
39.5	124	74	MED
40.3	188	15	SM GW
41.0	181	29	MEDGW
41.4	227	67	MED
42.2	76	67	MED
42.7	83	77	MED
47.0	341	89	MED
48.2	284	77	MED
48.4	284	71	MED
50.8	119	56	MED
51.4	282	70	MED
52.2	271	67	MED
53.9	345	16	MED GW
58.5	247	20	SM GW
59.4	267	39	MED
59.8	270	40	SM
60.1	269	36	SM
61.8	207	11	SM GW
62.4	356	13	SM GW
67.9	171	5	SM
67.9	142	7	MED GW

Appendix. Depth, dip azimuth, and dip angle of fractures and foliation observed by optical televiewer in five boreholes (W34ST-B, W37ST-A, W55ST-A, W26ST-A, and GroveST-A), Manhattan Island, N.Y., 2000-01--continued

Depth	Dip azimith, in degrees	Dip angle, in degrees	Fracture size
69.5	295	35	SM
71.9	133	9	SM GW
73.3	49	9	SM GW
78.9	19	3	MED
78.9	277	3	MED
79.5	156	12	LG
79.6	114	2	MED
80.8	169	12	MED GW
82.9	114	27	MED GW
90.5	249	10	SM
96.4	149	15	MED
97.8	236	19	SM
98.5	123	16	LG
99.5	137	3	LG
99.7	107	16	MED
100.2	267	32	MED
103.3	108	75	SM
104.4	78	11	SM
104.9	104	73	MED
106.5	255	16	MED
106.6	308	15	SM
107.1	130	8	SM
107.2	233	18	MED
107.4	193	31	SM
109.1	112	78	MED
111.9	65	9	SM
114.4	245	11	SM
114.7	190	19	SM
115.2	270	80	SM
116.9	111	84	SM
117.4	273	85	SM
119.3	70	9	MED
119.6	242	35	SM
119.7	89	78	SM
120.6	105	10	SM
124.7	353	7	SM
128.0	307	9	SM
133.8	254	62	SM
134.2	345	10	SM
134.4	249	36	MED
137.3	201	22	MED
138.9	248	34	SM
141.5	229	21	SM
141.9	224	22	MED
141.9	209	16	MED
142.3	225	20	MED
161.5	132	15	SM
161.6	144	5	MED
161.7	107	5	MED
163.0	270	3	SM
163.3	164	8	SM
171.8	126	20	SM
172.4	81	6	SM
173.9	46	14	MED
173.9	49	18	MED
177.4	90	22	SM
177.8	252	39	SM
178.5	57	13	SM
179.0	253	5	SM
179.0	139	8	MED
179.0	108	2	MED
184.1	323	15	SM
184.2	296	12	SM
184.5	273	12	SM
184.7	289	26	SM
210.5	323	18	SM
211.2	304	19	SM
214.8	277	32	MED
217.7	293	23	SM
219.6	267	25	SM
221.1	73	11	SM
221.3	27	11	SM
225.3	310	9	SM
228.0	288	67	SM
228.6	304	77	SM
229.9	338	14	SM
232.5	67	24	SM
233.7	34	5	MED
233.8	43	10	MED
239.5	316	3	SM
243.6	274	75	SM
264.2	70	12	SM
265.2	277	67	SM
275.1	290	74	SM
287.4	309	5	SM
289.5	17	11	SM
289.9	3	11	SM
290.0	337	9	MED

Appendix. Depth, dip azimuth, and dip angle of fractures and foliation observed by optical televiewer in five boreholes (W34ST-B, W37ST-A, W55ST-A, W26ST-A, and GroveST-A), Manhattan Island, N.Y., 2000-01--continued

Depth	Dip azimith, in degrees	Dip angle, in degrees	Fracture size
290.2	35	57	MED
290.5	53	50	MED
291.3	38	46	SM
291.9	269	72	SM
302.1	10	11	SM
316.5	268	71	MED
324.0	261	72	MED
333.2	283	13	SM
333.3	18	3	SM
337.7	279	48	MED
337.9	47	15	SM
342.3	254	5	MED
342.3	226	10	MED
344.0	281	14	SM
347.7	308	5	SM
347.7	34	5	SM
351.2	125	9	SM
351.2	269	29	MED
359.4	126	13	SM
360.7	70	13	SM
363.7	174	19	SM
364.4	160	56	MED
365.1	304	81	SM
367.0	83	34	SM
367.2	83	37	SM
367.4	92	50	MED
368.5	90	31	SM
368.8	20	14	SM
369.6	290	84	SM
370.0	329	27	SM
370.1	328	19	MED
370.2	351	79	MED
370.3	341	21	MED
370.3	342	19	SM
370.5	341	76	MED
370.7	328	76	SM
378.0	330	74	MED
378.0	333	73	MED
378.1	327	71	MED
378.9	334	9	MED
379.8	47	13	SM
380.0	124	2	MED
380.0	186	4	MED
380.7	337	71	MED
380.7	297	8	SM
381.2	123	31	SM
381.4	341	36	MED
381.5	293	66	MED
381.8	355	39	SM
382.2	325	57	MED
382.2	297	50	SM
382.4	79	19	MED
382.5	56	17	MED
382.5	312	63	MED
382.8	57	23	SM
382.9	54	13	MED
383.1	331	22	MED
383.3	134	24	SM
383.5	309	62	MED
383.7	294	32	SM
383.8	291	30	SM
383.9	317	34	MED
384.0	320	40	MED
384.0	307	61	MED
384.2	308	28	MED
384.3	148	15	SM
384.3	308	35	MED
384.7	193	8	MED
384.9	234	10	MED
384.9	114	36	MED
384.9	147	69	MED
385.1	270	26	MED
385.2	281	22	LG GW
385.7	103	63	MED
386.2	28	33	SM
386.6	253	43	MED
387.8	305	9	SM
387.8	126	31	SM
389.0	50	47	SM FLT
389.4	9	74	SM
389.5	2	81	SM
394.1	273	55	MED
399.0	347	31	SM
401.7	125	7	SM
402.0	265	29	SM
402.2	278	13	SM
402.8	96	83	MED
403.0	269	53	LG

Appendix. Depth, dip azimuth, and dip angle of fractures and foliation observed by optical televiewer in five boreholes (W34ST-B, W37ST-A, W55ST-A, W26ST-A, and GroveST-A), Manhattan Island, N.Y., 2000-01--continued

Depth	Dip azimith, in degrees	Dip angle, in degrees	Fracture size
403.5	261	88	MED
404.3	284	65	MED
404.4	302	64	MED
404.5	287	70	MED
405.5	168	15	SM
405.7	58	3	SM
405.9	55	12	SM
406.0	52	20	SM
406.0	164	6	SM
407.6	138	33	SM
408.2	281	64	SM
410.6	350	84	SM
410.9	123	5	SM
411.2	175	9	SM
411.4	54	34	SM
411.6	0	80	SM
412.4	342	85	MED
412.9	31	8	SM
428.5	341	81	SM
430.6	252	57	SM
431.2	245	58	SM
436.2	142	55	SM
437.2	284	35	SM
439.9	261	86	SM
441.2	35	7	SM
441.4	88	38	SM
443.8	355	82	MED
446.8	121	24	SM
449.0	109	15	SM
449.9	123	20	SM
450.9	114	16	MED
466.9	279	65	SM
473.3	300	45	SM
475.9	296	62	SM
483.9	296	54	SM
499.4	305	40	SM
500.6	271	51	MED
501.7	264	67	SM
513.2	301	32	SM
514.0	294	46	SM
624.3	321	16	SM
Foliation			
30.7	248	60	
36.1	275	64	
55.9	245	60	
60.0	282	42	
64.6	294	45	
67.8	242	59	
69.5	298	39	
77.9	283	53	
100.5	69	76	
102.4	93	62	
105.1	67	70	
109.0	108	78	
117.9	106	82	
128.5	129	58	
133.8	250	62	
134.5	252	59	
135.3	258	62	
137.3	222	59	
138.6	201	30	
159.1	280	52	
160.1	259	65	
161.6	257	76	
178.8	211	36	
181.2	247	40	
182.5	217	31	
184.2	282	31	
184.9	239	23	
206.9	274	63	
209.2	272	69	
214.6	290	32	
219.7	278	34	
221.0	254	61	
221.8	279	30	
224.7	288	21	
225.6	242	41	
227.3	278	27	
231.2	275	74	
233.5	64	62	
255.0	270	63	
263.9	287	69	
265.8	282	79	
275.4	289	64	
278.5	298	80	
281.7	271	69	
290.2	283	82	
291.7	276	67	

Appendix. Depth, dip azimuth, and dip angle of fractures and foliation observed by optical televiewer in five boreholes (W34ST-B, W37ST-A, W55ST-A, W26ST-A, and GroveST-A), Manhattan Island, N.Y., 2000-01--continued

Depth	Dip azimith, in degrees	Dip angle, in degrees	Fracture size
296.9	276	72	
316.9	278	58	
320.3	272	69	
324.8	293	55	
337.5	287	60	
354.9	286	67	
365.7	152	42	
367.0	89	29	
370.0	327	25	
384.1	306	51	
386.5	276	35	
388.6	260	47	
390.8	253	57	
394.0	266	55	
397.0	270	59	
404.9	280	55	
406.4	268	64	
408.7	279	67	
416.8	259	64	
421.3	256	65	
430.6	244	55	
461.2	274	55	
462.8	282	56	
466.1	282	53	
469.6	319	31	
471.9	303	48	
475.0	277	63	
477.3	315	50	
483.0	268	57	
485.2	292	61	
487.5	281	64	
492.2	309	37	
509.3	319	41	
511.4	307	27	
512.6	304	34	
520.2	278	26	
523.1	308	47	
526.2	279	44	
532.5	281	59	
534.1	279	46	
538.9	291	43	
544.4	241	29	
548.3	279	30	
551.0	263	18	
554.9	306	29	
556.9	268	42	
558.1	279	53	
561.6	276	48	
571.9	294	63	
575.3	286	56	
582.1	295	56	
589.9	284	68	
590.9	265	64	
599.0	295	71	
600.3	282	68	
605.3	278	66	
608.4	276	74	
609.9	287	64	
612.4	288	83	
625.0	272	80	
633.1	277	73	
639.1	301	83	
641.3	279	72	
W55ST-A			
Fractures			
161.8	61	14	SM
162.4	303	63	MED
166.4	20	36	MED
169.9	130	21	MED
173.1	129	22	SM
173.5	38	34	MED
179.8	287	61	SM
180.5	300	64	SM
183.1	137	7	SM
198.4	61	39	SM
199.2	122	28	SM
200.7	295	72	SM
201.3	303	25	MED
201.5	294	74	MED
201.5	301	11	SM
204.7	308	60	SM
205.3	285	58	SM
211.0	292	68	SM
212.9	292	61	SM
222.0	302	52	SM
224.5	292	64	SM
225.0	294	58	SM
225.2	296	66	SM

Appendix. Depth, dip azimuth, and dip angle of fractures and foliation observed by optical televiewer in five boreholes (W34ST-B, W37ST-A, W55ST-A, W26ST-A, and GroveST-A), Manhattan Island, N.Y., 2000-01--continued

Depth	Dip azimith, in degrees	Dip angle, in degrees	Fracture size
225.4	290	65	SM
225.7	301	58	SM
226.6	54	15	MED
230.2	305	60	SM
230.9	178	76	MED
234.4	286	66	SM
240.0	267	7	SM
251.2	58	23	SM
251.2	71	23	MED
251.8	287	44	SM
259.4	286	65	SM
265.1	54	39	SM
265.8	52	48	MED
266.3	284	64	MED
268.1	264	56	SM
279.3	274	56	SM
279.8	259	52	SM
283.9	95	43	SM
285.9	43	73	SM
290.8	73	6	SM
296.4	36	5	SM
296.4	190	3	SM
314.7	125	50	SM
329.3	263	14	SM
329.5	117	17	SM
330.1	137	17	MED
333.5	70	13	SM
335.2	270	43	SM
335.2	77	27	SM
335.5	288	47	SM
335.6	270	65	SM
335.6	113	4	MED
335.7	77	22	LG
335.9	299	35	MED
336.0	78	10	MED
336.4	282	57	LG
336.9	281	59	SM
337.1	281	58	SM
340.3	270	65	SM
361.5	35	29	SM
367.6	295	33	SM
376.4	296	68	SM
377.6	164	75	MED
379.0	181	76	SM
379.2	258	67	MED
379.4	172	71	LG
383.9	300	70	LG
386.0	289	62	MED
390.3	292	48	SM
392.4	302	68	SM
395.4	285	60	MED
431.2	288	54	SM
431.7	297	18	SM
431.8	297	67	SM
432.1	285	32	SM
432.3	299	43	SM
432.4	255	64	SM
434.6	292	59	SM
436.1	255	2	SM
455.5	301	57	SM
460.5	214	72	SM
468.4	296	50	SM
468.6	296	49	SM
470.3	293	50	SM
471.2	285	53	SM
483.5	166	6	SM
484.8	256	10	SM
485.1	249	50	SM
485.4	124	32	MED
485.5	241	44	SM
489.1	261	51	SM
490.5	266	32	SM
490.7	265	45	MED
490.7	262	45	MED
492.0	221	70	MED
492.9	269	61	MED
493.8	298	59	SM
502.7	231	74	SM
511.2	262	66	SM
523.7	143	6	SM
530.8	294	55	SM
542.1	311	67	MED
542.9	297	61	MED
544.1	291	65	SM
544.9	300	58	SM
552.8	311	60	SM
553.2	299	47	SM
577.0	67	61	SM

Appendix. Depth, dip azimuth, and dip angle of fractures and foliation observed by optical televiewer in five boreholes (W34ST-B, W37ST-A, W55ST-A, W26ST-A, and GroveST-A), Manhattan Island, N.Y., 2000-01--continued

Depth	Dip azimith, in degrees	Dip angle, in degrees	Fracture size
577.8	91	67	SM
578.5	318	58	SM
579.1	80	39	SM
582.7	319	68	SM
585.7	304	48	MED
586.4	279	61	MED
591.8	301	25	SM
598.2	293	66	MED
600.3	303	52	SM
601.0	69	55	MED
605.1	270	66	LG
606.4	267	50	SM
607.8	301	54	SM
608.3	309	49	SM
611.7	197	53	SM
616.4	130	80	MED
Foliation			
166.5	311	50	
176.8	281	65	
177.6	276	67	
180.6	297	72	
183.6	296	65	
184.6	303	56	
186.8	300	66	
188.3	295	61	
190.0	306	66	
194.0	296	66	
196.1	283	50	
197.3	289	72	
199.1	291	71	
201.5	288	73	
203.4	306	69	
205.3	291	65	
209.6	283	72	
212.9	283	59	
216.7	281	64	
219.4	284	60	
223.8	292	65	
225.4	291	65	
228.7	278	57	
233.4	283	66	
236.2	282	62	
239.8	273	73	
241.2	277	62	
244.8	272	67	
248.5	311	54	
251.1	281	60	
257.3	278	60	
260.4	280	66	
265.0	286	76	
268.2	265	65	
271.6	274	65	
275.3	281	57	
280.1	266	53	
280.8	280	50	
284.3	291	61	
287.4	288	65	
291.3	302	61	
295.2	294	67	
297.9	286	63	
301.5	284	68	
304.9	290	47	
308.1	289	53	
310.5	292	66	
312.7	291	73	
315.5	287	68	
317.1	285	63	
318.0	265	56	
319.7	290	70	
321.9	287	52	
327.1	274	54	
328.7	283	56	
330.5	283	52	
332.7	267	61	
334.9	288	49	
337.5	273	58	
340.5	281	69	
342.9	270	61	
347.6	285	63	
350.2	283	55	
353.3	287	51	
354.1	283	47	
355.8	285	38	
358.4	275	44	
359.9	278	59	
361.6	289	64	
365.0	283	55	
366.7	278	40	

Appendix. Depth, dip azimuth, and dip angle of fractures and foliation observed by optical televiewer in five boreholes (W34ST-B, W37ST-A, W55ST-A, W26ST-A, and GroveST-A), Manhattan Island, N.Y., 2000-01--continued

Depth	Dip azimith, in degrees	Dip angle, in degrees	Fracture size
368.4	281	36	
370.1	273	55	
371.9	283	67	
377.6	282	67	
381.0	269	62	
383.5	289	56	
386.8	276	53	
388.2	269	56	
389.7	288	57	
393.1	292	50	
393.8	280	56	
395.1	280	56	
396.8	283	65	
400.3	279	55	
401.8	282	61	
405.2	273	62	
407.7	285	36	
412.8	285	32	
414.7	301	49	
418.6	290	67	
420.5	288	62	
422.7	292	52	
424.5	287	58	
426.0	295	59	
429.0	288	62	
433.6	287	59	
436.6	285	62	
444.6	277	59	
448.1	286	45	
452.1	284	57	
455.0	285	60	
457.4	282	68	
461.5	281	68	
464.4	286	65	
465.9	283	60	
466.8	281	54	
467.4	281	51	
471.0	285	56	
476.5	298	68	
477.3	275	54	
483.5	274	79	
485.1	235	46	
488.6	268	67	
490.7	260	53	
492.9	270	60	
493.8	288	58	
494.5	281	51	
520.9	319	66	
522.9	312	68	
530.8	290	55	
532.3	299	62	
533.9	296	60	
537.4	302	56	
538.6	303	57	
541.3	303	56	
543.1	302	55	
544.8	293	62	
547.7	293	60	
550.7	295	65	
552.7	289	61	
556.1	284	64	
558.1	293	70	
561.2	286	67	
565.5	284	71	
568.7	274	62	
581.5	326	63	
582.7	320	69	
585.7	301	59	
586.7	298	74	
589.8	289	68	
594.8	285	70	
596.3	287	60	
597.6	299	62	
599.2	289	59	
602.6	288	58	
605.7	274	67	
607.9	279	58	
609.3	299	58	
611.1	300	52	
614.5	289	62	
W26ST-A			
Fractures			
45.11	249	33	SM
45.93	86	21	MED
48.36	258	33	SM
52.14	267	19	MED
53.36	247	64	SM
54.15	248	51	SM

Appendix. Depth, dip azimuth, and dip angle of fractures and foliation observed by optical televiewer in five boreholes (W34ST-B, W37ST-A, W55ST-A, W26ST-A, and GroveST-A), Manhattan Island, N.Y., 2000-01--continued

Depth	Dip azimith, in degrees	Dip angle, in degrees	Fracture size
54.69	258	58	SM
56.86	251	70	LG
57.86	254	63	MED
59.93	297	8	SM
60.44	286	66	SM
61.95	251	42	MED
63.21	244	61	SM
63.45	231	37	SM
64.15	126	6	SM
64.2	138	8	MED
90.04	260	48	SM
90.74	99	57	SM
91.09	98	34	SM
91.48	269	54	MED
93.55	318	66	SM
93.85	327	69	MED
94.33	265	48	MED
96.59	335	23	SM
101.86	59	3	SM
103.84	88	26	MED
105.53	284	33	SM
108.4	266	59	SM
117.89	270	63	SM
118.39	267	61	SM
118.8	266	57	MED
124.46	272	53	SM
127.6	265	51	SM
129.53	274	52	SM
130.53	249	10	MED
131.91	303	10	SM
132.05	288	35	MED
136.78	270	6	MED
137.32	87	21	SM
137.2	122	28	MED
138.58	162	80	MED
152.64	350	38	MED
152.93	129	40	MED
153.14	285	54	MED
154.94	305	36	SM
155.11	290	31	SM
157.17	324	40	MED
162.37	263	25	SM
167.27	6	13	MED
167.37	270	23	MED
167.43	45	16	SM
171.04	270	37	MED
171.89	198	36	MED
182.59	51	52	SM FLT
183.12	204	8	SM
198.59	222	29	MED
215.68	174	62	SM
220.62	167	89	MED
222.83	282	48	MED
225.77	282	47	SM
227.26	70	23	MED
227.38	281	49	SM
227.64	116	7	SM
228.92	284	49	SM
230.02	283	47	SM
230.36	106	26	MED
230.66	278	42	MED
242.69	155	84	MED
254.8	285	63	SM
257.37	284	64	SM
258.19	57	22	SM
258.33	77	16	MED
259.15	282	65	MED
259.54	271	79	MED
261.19	288	64	MED
262.39	246	23	MED
263.4	288	46	SM
263.3	292	50	MED
264.05	241	14	SM
266.28	282	66	MED GW
268.85	310	23	MED
268.96	261	33	MED
269.32	1	21	MED
269.4	326	24	MED
269.52	355	3	MED
269.52	152	24	MED
269.62	133	16	MED
269.78	170	46	LG
270.26	195	10	VLG
270.34	162	35	VLG
270.98	111	27	VLG
271.26	86	23	VLG
271.54	3	37	VLG
271.81	279	24	VLG

Appendix. Depth, dip azimuth, and dip angle of fractures and foliation observed by optical televiewer in five boreholes (W34ST-B, W37ST-A, W55ST-A, W26ST-A, and GroveST-A), Manhattan Island, N.Y., 2000-01--continued

Depth	Dip azimith, in degrees	Dip angle, in degrees	Fracture size
271.88	318	4	MED
272.01	284	6	MED
272.55	157	19	LG
273.08	354	86	MED
272.81	75	4	MED
274.02	175	15	MED
274.09	287	25	MED
274.39	301	36	MED
274.59	283	49	MED
274.62	104	25	MED
274.95	47	15	LG
275.1	309	40	LG
275.14	312	41	LG
275.22	142	40	MED
275.44	116	42	MED
275.59	173	31	MED
275.96	277	37	LG
276.08	224	16	LG
276.16	177	33	MED
276.49	237	71	MED
276.49	314	71	LG
276.89	67	24	LG
276.94	82	22	LG
277.05	109	68	MED
277.55	24	19	LG
277.84	81	4	MED
277.88	73	4	MED
277.92	308	12	MED
278.35	54	16	SM
278.47	311	33	SM
278.54	15	6	MED
278.74	263	7	SM
278.76	228	11	MED
279.19	200	14	MED
279.65	282	46	MED
280.13	307	53	SM
279.98	301	45	LG
280.51	232	8	MED
281.45	243	22	SM
281.69	256	26	MED
282.97	326	72	SM
283.52	303	51	SM
288.36	272	42	MED
291.05	276	57	LG
295.98	281	50	SM
296.14	255	55	SM
297.28	192	67	SM
297.22	269	43	SM
299.3	287	31	SM
298.93	291	26	SM
303.26	59	55	SM
305.05	99	89	SM
309.02	268	76	SM
311.46	306	24	SM
311.5	291	25	SM
311.62	310	21	MED GW
311.94	295	12	SM
312.0	259	14	MED
313.0	9	61	SM
313.19	291	23	SM
313.22	283	22	MED GW
314.04	326	19	SM
317.3	295	20	SM
317.33	285	19	MED
323.41	251	37	SM
335.31	121	46	SM
335.47	57	53	MED
336.31	132	68	SM
349.18	255	29	MED
349.21	266	37	MED
349.28	267	35	SM
360.61	164	74	SM
396.22	329	37	SM
397.65	109	78	SM FLT
404.06	287	46	MED
412.35	43	66	SM FLT
414.4	113	18	MED
422.58	74	22	SM
428.03	201	14	MED
429.56	274	61	SM
430.21	274	65	MED
430.5	289	18	MED
430.79	267	17	MED
434.52	278	68	MED
440.15	114	14	SM
443.05	267	27	SM
443.16	269	24	SM
443.32	263	37	MED

Appendix. Depth, dip azimuth, and dip angle of fractures and foliation observed by optical televiewer in five boreholes (W34ST-B, W37ST-A, W55ST-A, W26ST-A, and GroveST-A), Manhattan Island, N.Y., 2000-01--continued

Depth	Dip azimith, in degrees	Dip angle, in degrees	Fracture size
447.86	211	13	SM
448.03	223	25	SM
447.57	185	8	SM
495.32	282	32	SM
497.79	296	12	SM
498.01	291	17	SM
498.84	276	26	SM
504.13	283	29	SM
521.61	92	29	SM
523.86	90	34	SM
523.97	74	46	SM
532.8	59	14	SM
532.87	306	55	SM
544.33	43	47	SM
553.9	282	3	SM
567.59	271	55	SM
577.96	353	2	SM
Foliation			
42.1	236	64	
46.01	246	59	
47.11	243	63	
50.68	254	67	
55.08	253	68	
57.21	249	53	
59.1	268	70	
65.28	273	74	
68.23	268	77	
72.65	252	79	
75.62	266	72	
77.19	258	71	
80.54	248	70	
82.66	259	75	
87.98	247	57	
90.04	257	49	
93.04	269	46	
95.11	278	47	
107.76	281	52	
110.89	271	56	
114.99	264	60	
117.89	270	61	
119.23	271	54	
120.44	266	44	
122.09	274	48	
124.58	272	56	
125.99	270	53	
127.01	275	50	
128.5	261	55	
129.53	274	53	
131.44	276	57	
132.92	276	51	
134.89	281	49	
136.32	277	52	
140.51	100	49	
148.79	292	51	
150.84	279	51	
154.27	288	54	
155.1	281	34	
157.58	290	58	
158.51	295	47	
161.87	272	46	
166.32	310	72	
173.93	276	67	
177.37	279	62	
184.87	275	53	
188.46	310	67	
191.49	309	74	
192.45	308	57	
194.38	310	53	
197.42	294	60	
202.08	284	55	
206.68	308	46	
208.32	306	60	
221.24	273	48	
222.59	285	52	
224.04	279	45	
225.48	275	53	
228.02	288	58	
230.03	289	48	
234.13	302	59	
246.72	281	60	
250.27	296	66	
253.9	283	65	
256.46	291	60	
262.82	305	50	
266.63	292	57	
268.5	291	41	
289.43	277	53	
292.39	274	51	

Appendix. Depth, dip azimuth, and dip angle of fractures and foliation observed by optical televiewer in five boreholes (W34ST-B, W37ST-A, W55ST-A, W26ST-A, and GroveST-A), Manhattan Island, N.Y., 2000-01--continued

Depth	Dip azimith, in degrees	Dip angle, in degrees	Fracture size
295.69	283	52	
297.21	275	43	
299.15	283	44	
300.35	279	48	
302.4	191	20	
303.0	227	32	
309.17	288	66	
314.62	281	83	
320.95	119	74	
323.45	121	67	
330.97	309	47	
334.89	345	31	
347.5	287	66	
360.26	298	58	
400.25	307	54	
403.41	295	37	
407.16	294	55	
410.15	288	65	
412.73	299	55	
418.21	285	61	
420.55	304	62	
425.55	264	59	
429.55	274	59	
435.34	274	61	
436.53	292	70	
451.91	290	82	
454.8	295	75	
457.35	291	71	
459.26	271	70	
461.87	294	79	
466.97	303	67	
469.3	294	86	
472.18	288	73	
474.18	273	67	
478.8	274	58	
480.55	285	83	
485.07	290	84	
488.84	310	88	
497.46	307	84	
505.61	285	69	
508.1	305	49	
508.92	297	61	
511.21	303	59	
512.03	306	57	
516.61	268	71	
518.73	279	59	
534.76	285	60	
537.33	99	69	
540.85	294	75	
544.34	284	67	
546.16	259	80	
548.06	286	80	
552.11	281	83	
556.62	291	82	
557.9	276	76	
562.35	298	87	
564.0	287	73	
565.18	286	72	
566.01	284	67	
567.41	284	68	
568.92	287	62	
569.55	290	69	
570.75	271	65	
572.5	275	61	
573.77	287	67	
575.15	284	78	
578.0	298	74	
579.76	279	76	
582.23	281	75	
583.8	286	56	
585.28	288	56	
GroveST-A			
Fractures			
83.41	170	19	VLG
83.53	204	20	VLG
84.56	291	39	MED
86.01	259	38	MED
95.11	357	18	SM
95.11	298	17	SM
96.97	85	17	SM
96.93	87	15	SM
109.35	93	19	SM
110.57	77	9	SM
111.27	281	14	MED
113.53	26	21	MED
113.56	88	9	SM
113.61	135	9	MED
114.85	124	24	MED

Appendix. Depth, dip azimuth, and dip angle of fractures and foliation observed by optical televiewer in five boreholes (W34ST-B, W37ST-A, W55ST-A, W26ST-A, and GroveST-A), Manhattan Island, N.Y., 2000-01--continued

Depth	Dip azimith, in degrees	Dip angle, in degrees	Fracture size
115.33	303	14	SM
115.86	280	5	MED
116.0	209	7	SM
117.68	49	2	MED
118.39	298	29	SM
118.49	274	26	SM
119.36	70	24	SM
119.55	152	25	SM
119.75	136	6	SM
120.05	244	19	SM
120.17	299	28	MED
120.34	80	37	MED
120.59	281	58	MED
120.95	343	14	SM
120.88	307	29	SM
120.55	279	86	MED
121.95	283	59	MED
123.06	102	26	SM
129.64	44	7	SM
129.68	65	11	SM
134.66	294	33	SM
142.45	89	26	SM
143.45	126	24	SM
145.28	253	24	SM
149.17	264	22	SM
150.79	285	73	MED
152.74	277	37	MED
153.88	278	11	MED
153.94	122	14	MED
154.79	130	14	SM
156.08	269	16	MED
156.49	298	14	LG
156.66	54	12	MED
156.71	133	3	SM
157.09	276	58	SM
156.92	281	52	SM
157.51	286	72	MED
158.1	312	39	SM
162.04	310	30	SM
163.64	299	39	MED
164.22	119	11	LG
164.38	151	29	MED
168.4	102	16	MED
168.6	94	16	MED
168.86	304	13	SM
169.46	271	62	SM
171.89	247	19	SM
174.16	271	43	MED
175.47	336	16	SM
179.8	127	17	SM
181.06	291	31	SM
183.14	10	59	SM
184.13	154	2	SM
185.02	304	13	SM
185.29	51	48	SM
185.39	355	31	SM
185.52	346	19	SM
186.31	305	11	SM
186.5	32	7	SM
186.71	2	26	SM
187.39	296	48	LG
190.03	264	27	SM
196.48	154	4	SM
200.76	304	18	SM
202.21	126	9	SM
209.19	290	42	MED
212.67	302	65	SM
213.57	121	22	SM
213.88	76	39	SM
225.62	69	13	SM
225.65	25	10	SM
244.18	244	15	SM
252.82	52	18	SM
257.06	122	73	MED
262.42	338	33	SM
265.29	356	26	SM
269.04	314	49	SM
269.07	296	9	MED
270.74	18	32	SM
270.88	113	28	SM
286.52	300	44	SM
286.91	285	45	SM
294.69	288	57	SM
295.7	311	38	SM
296.14	287	58	SM
299.24	297	55	MED
304.13	302	34	LG
305.57	290	49	SM

Appendix. Depth, dip azimuth, and dip angle of fractures and foliation observed by optical televiewer in five boreholes (W34ST-B, W37ST-A, W55ST-A, W26ST-A, and GroveST-A), Manhattan Island, N.Y., 2000-01--continued

Depth	Dip azimith, in degrees	Dip angle, in degrees	Fracture size
306.09	281	67	MED
307.47	293	62	MED
309.71	18	20	MED
310.7	290	51	SM
311.58	128	47	SM
311.6	299	35	SM
312.02	292	67	SM
312.29	285	58	SM
312.51	287	45	SM
312.89	295	62	SM
313.37	295	48	SM
313.64	298	29	SM
314.04	301	53	SM
319.02	297	39	MED
324.25	195	52	SM
330.52	302	40	MED
334.71	99	81	MED
338.88	286	84	LG
339.53	288	73	MED
340.01	274	78	LG
340.45	290	59	MED
342.94	93	6	MED
348.09	336	30	SM
348.71	312	47	MED
358.42	302	47	MED
359.04	281	41	MED
360.26	300	14	SM
360.37	92	44	MED
360.4	184	24	SM
360.54	309	37	SM
360.82	222	23	SM
360.81	61	53	SM
360.96	146	47	MED
361.81	295	38	MED
361.96	144	43	SM
362.06	305	33	SM
362.77	177	48	SM
363.51	287	40	MED
363.94	175	63	SM
365.45	288	74	MED
368.46	298	71	SM
369.43	290	72	MED
373.07	132	29	MED
373.14	294	71	MED
374.47	356	4	SM
374.49	295	8	SM
378.87	292	74	SM
379.91	291	73	SM
382.23	294	70	SM
382.65	291	79	SM
383.5	282	75	SM
387.28	151	14	SM
389.2	289	84	SM
389.44	291	84	MED
390.6	155	2	SM
390.96	139	29	SM
392.52	159	2	SM
393.42	292	58	MED
394.32	23	6	SM
397.34	180	36	SM
401.04	280	24	MED
421.28	39	3	MED
426.7	316	29	SM
430.88	311	42	SM
436.61	96	79	MED
439.88	32	8	SM
440.83	285	67	MED
440.95	284	68	MED
441.24	275	75	SM
449.35	278	83	MED
456.21	292	49	MED
458.31	292	74	SM
462.17	281	75	LG
462.3	282	80	LG
464.96	307	56	MED
469.2	321	24	SM
470.69	271	74	VLG
471.66	126	11	SM
475.33	102	87	MED
477.37	301	71	MED
478.72	286	60	SM
482.08	304	24	MED
484.88	110	85	MED
493.75	191	5	MED
494.48	288	47	MED
495.81	345	5	SM
495.93	359	13	SM
496.14	357	6	SM

Appendix. Depth, dip azimuth, and dip angle of fractures and foliation observed by optical televiewer in five boreholes (W34ST-B, W37ST-A, W55ST-A, W26ST-A, and GroveST-A), Manhattan Island, N.Y., 2000-01--continued

Depth	Dip azimith, in degrees	Dip angle, in degrees	Fracture size
496.26	116	7	SM
496.48	195	12	SM
497.42	353	3	SM
497.44	191	18	MED
497.93	122	21	MED
520.7	268	8	MED
525.9	333	25	SM
526.07	341	23	SM
530.78	313	46	LG
531.04	289	58	MED
532.25	320	70	MED
532.84	324	68	MED
536.94	56	53	VLG
535.68	188	74	VLG
534.52	271	87	VLG
540.36	301	80	LG
539.79	264	15	MED
541.45	324	5	LG
541.11	322	71	VLG
548.16	355	12	SM
548.09	319	22	MED
548.09	319	22	MED
549.51	295	83	SM
555.22	293	35	SM
556.94	293	38	SM
557.08	302	28	SM
557.17	330	18	SM
557.25	298	14	MED
558.0	159	24	SM
558.11	199	17	SM
564.12	105	88	SM FLT
565.29	285	66	SM
573.7	244	36	MED
598.96	302	41	MED
605.98	303	39	MED
608.11	291	63	MED
607.65	302	61	MED
608.48	299	51	MED
606.69	141	82	SM
610.86	309	49	SM
614.67	301	65	SM
614.65	149	77	SM
615.53	75	27	SM
615.35	294	76	MED
616.41	326	21	SM
616.8	332	32	SM
618.13	46	16	SM
618.35	355	11	SM
619.74	304	54	MED
621.03	297	50	SM
621.39	93	41	SM
623.26	295	54	SM
623.75	84	31	MED
626.83	348	30	MED
628.88	301	32	MED
Foliation			
163.02	278	40	
164.43	283	73	
167.42	265	79	
171.52	105	37	
173.55	119	71	
179.81	100	73	
181.35	95	66	
186.07	89	77	
195.68	278	86	
199.91	287	82	
219.83	290	85	
223.51	288	43	
224.22	294	48	
236.81	303	34	
237.55	284	24	
242.73	44	16	
244.47	272	18	
246.24	50	22	
249.27	111	59	
250.6	289	22	
257.6	108	78	
259.32	93	78	
264.1	284	76	
266.37	299	75	
271.64	285	74	
274.8	306	56	
276.22	273	79	
277.1	289	13	
280.13	288	63	
284.18	288	29	
286.8	309	49	
290.44	309	44	

Appendix. Depth, dip azimuth, and dip angle of fractures and foliation observed by optical televiewer in five boreholes (W34ST-B, W37ST-A, W55ST-A, W26ST-A, and GroveST-A), Manhattan Island, N.Y., 2000-01--continued

Depth	Dip azimith, in degrees	Dip angle, in degrees	Fracture size
291.93	298	37	
293.97	305	43	
295.7	304	36	
296.34	303	40	
302.21	281	86	
307.09	302	47	
311.5	289	38	
313.38	299	46	
313.86	302	28	
315.23	288	51	
315.91	80	38	
318.83	288	63	
319.73	303	41	
322.9	305	16	
325.99	90	37	
328.86	285	44	
332.97	293	55	
335.67	103	61	
339.85	281	71	
343.15	296	44	
343.94	301	57	
345.69	292	66	
350.61	296	45	
354.76	312	42	
358.81	298	64	
361.38	302	38	
362.9	301	32	
364.79	293	36	
369.14	289	79	
371.95	286	84	
376.43	289	82	
379.2	271	76	
381.17	283	78	
383.49	283	80	
385.09	288	79	
388.06	287	83	
393.62	291	82	
395.82	296	82	
399.61	276	84	
411.17	299	87	
420.97	283	85	
423.92	305	86	
430.89	301	39	
438.4	295	85	
441.27	272	74	
447.82	276	79	
450.47	286	81	
458.33	293	76	
461.28	284	84	
463.12	293	81	
465.83	304	46	
467.7	296	82	
477.41	305	68	
485.52	275	87	
494.55	131	40	
497.52	282	86	
508.9	338	61	
522.34	286	88	
543.18	274	76	
550.06	280	86	
552.6	274	80	
557.46	285	80	
559.48	286	81	
566.2	279	77	
574.54	91	88	
599.85	294	41	
608.78	297	59	
609.97	298	46	
611.51	296	55	
615.95	286	77	
622.48	291	64	
623.62	295	39	
630.68	101	65	
632.76	104	62	
633.35	111	48	
599.85	294	41	
608.78	297	59	
609.97	298	46	
611.51	296	55	
615.95	286	77	
622.48	291	64	
623.62	295	39	
630.68	101	65	
632.76	104	62	
633.35	111	48	